

List of changes to manuscript

February 11, 2016

We are thankful to the reviewers for the insightful suggestions and comments. Their comments and questions have led to various corrections of the manuscript. Additions are marked in blue in the attached version of the manuscript while deleted text is in red and struck through. Main changes are :

1. addition of a description of the microphysics scheme following the suggestions of the referees
2. addition of a table comparing bulk microphysical properties in the simulation with in situ observations (Table 2) following reviewer 1 and 3 requests
3. addition of a discussion on the sensitivity to nucleation-related parameters of the microphysics scheme and associated new figure (Figure 8) and Table (table 3)
4. minor changes in figure 1, 2, 3, 4 and 11 following the suggestion of reviewer 2
5. minor changes in figure 9 following the suggestion of reviewer 3

A modelling case study of a large-scale cirrus in the tropical tropopause layer

February 13, 2016

We would like to thank the reviewer for the insightful evaluation of our work. Please find below our point-by-point reply.

1. **Reviewer** — This paper describes simulations of a specific TTL cirrus event and provides useful insight into TTL cirrus physical processes and impacts on water vapor. The paper is interesting and well written. The paper should ultimately be suitable for publication in ACP, but I would like the authors to consider the following comments and suggestions. In particular, I would like to see more details about the WRF microphysics parameterizations used and the simulated cloud microphysical properties.

Authors — We agree with the referee that a description of the microphysics is necessary. This has been done following the referee’s suggestion in the Model description section (see also below). Also, to briefly address the sensitivity on specific microphysical parameters in the reference Thompson scheme, we have added a short discussion on those in subsection 4.2 on and one associated additional figure.

2. **Reviewer** — 1. Page 31091, first partial sentence: Suggest citing Wang et al. (1996, JGR). This paper reported SAGE measurements of TTL cirrus which provided the first indication of their high occurrence frequency.

Authors — Thank you for pointing out this reference, which we have added.

3. **Reviewer** — 2. Page 31091, lines 2-4: I think the extents to which TTL cirrus radiative heating affects the temperature and upwelling are not well known. What is clear is that the clouds affect the TTL thermal budget.

Authors — We agree. We have added a ‘potentially’ to this sentence to emphasize that it is a bit speculative.

4. **Reviewer** — 3. Page 31095, lines 6-7: Somewhere prior to this point (perhaps in the model description section), the authors should describe the ice nucleation scheme in the Thompson parameterization. Does the nucleation parameterization require substantial ice super-saturation for ice production (which would be consistent with homogeneous freezing of aqueous aerosols)? Are treatments of heterogeneous nucleation included? Are

mass- dimensional relationships used based on observations of cirrus at TTL temperatures or extrapolations from warmer temperatures?

Authors — A paragraph describing the microphysical assumptions in the Thompson scheme has been added in the text, on p6-7 of the revised manuscript. As explained, the parameterization involves a threshold supersaturation for nucleation to occur, which is much lower than the thresholds that would be relevant for homogeneous nucleation in a (single) air parcel. It could be interpreted as heterogeneous nucleation, but above all it is consistent with the scales of mesoscale modelling, i.e. it would produce unrealistic results to wait for the average supersaturation over a 10 km x 10 km x 300 m grid box to reach levels of 60% before triggering nucleation.

5. **Reviewer** — 4. Page 31095: What about the sensitivity of the ATB to ice crystal size distribution? I would hope that some comparison between the simulated effective radii and aircraft observations (Lawson et al., 2008; Kramer et al., 2009) is provided somewhere in the paper.

Authors — We have added a sentence mentioning the sensitivity to ice crystal size distribution; however, as now specified in the text, we have not carried any sensitivity study on this parameter to keep the consistency with the assumptions inside the microphysical code. See answer to the next question regarding the comparison with previous aircraft observations.

6. **Reviewer** — 5. Page 31096, lines 12-14: Despite the lack of microphysical cloud property observations for this particular cirrus event, it would still be useful to present the simulated cloud microphysical properties (ice water content, ice concentration, ice crystal size) and compare with statistics from previous observations (Lawson et al. and Kramer et al.).

Authors — We have added a Table (Table 2) summarizing the bulk microphysical properties of our cirrus field. We have also added near the end of section 2.3 a paragraph mentioning the comparison with Lawson et al. (2008) and Kramer et al. (2009).

7. **Reviewer** — 6. Page 31106, lines 4-5: The authors should also mention the Dinh et al. papers suggesting that radiative heating-induced internal cloud dynamics has a large impact on TTL cirrus evolution.

Authors — We have added the reference to those papers in this section.

8. **Reviewer** — 7. Page 31108, lines 10-20: In the discussion of cloud radiative heating rates for the simulated TTL cirrus system, it would be useful to know how typical the simulated cloud properties are for TTL cirrus. As suggest above, a comparison between the simulated microphysical properties and the typical values reported by Lawson et al. (2008) would be helpful in this respect.

Authors — We agree. At this point in the text, we have added a reference to the relevant section of the manuscript that compares the microphysical properties of our cirrus to observations.

9. **Reviewer** — 8. Page 31108, lines 24-25: It would be more accurate to say "...the magnitude of wind shear was found to be an important factor affecting the buildup of cloud-scale circulations..."

Authors — Corrected

10. **Reviewer** — 9. Pages 31109-31110: The authors make an important point here: that radiatively- induced cloud vertical motions have little impact on the cirrus evolution because (1) the lifetime of air parcels in the cloud system is too short, and (2) the induced vertical motions would be comparable to or smaller than the typical mesoscale motions present. Perhaps it would be worth mentioning this result in the abstract.

Authors — We have adopted the reviewer's suggestion and added a sentence in the abstract.

11. **Reviewer** — Figure 10: Most people working in the TTL clouds and water vapor field use ppmv. Figure 10 would be easier to quantitatively interpret if the authors used ppmv rather than ppm.

Authors — We have adopted the reviewer's suggestion and changed the units.

A modelling case study of a large-scale cirrus in the tropical tropopause layer

February 13, 2016

We would like to thank the reviewer for the insightful evaluation of our work. Please find below our point-by-point reply.

1. **Reviewer** — 1. Model set up: The set up of the model domain needs justification. The cloud formation along the south-east boundary (Figures 2, 3, 4, and 7) is probably spurious. It may be related to the large deviation from the analysis field of "up to 3 K at 16 km, 36 h after initialization" (page 31096, line 16). The comparison shown in Figure 7 indicates that the initialization by ERA Interim, rather than ECMWF operational analysis used for "reference simulation," has suffered less from this problem. Some expansion of the model domain may not solve this problem. Considering that the south-east boundary corresponds to the upstream of the cirrus clouds under consideration, it is necessary to examine the effect of the boundary carefully.

Authors — We understand the concern of the reviewer. Actually, the development of cirrus clouds in the South-East part of the domain is not entirely spurious; on earlier Calipso tracks, cirrus clouds are also seen in this region, as illustrated on figure 1 (included in this response, see below). It remains that the opacity of those clouds is likely overestimated by the model.

However, we expect that this only very marginally affects the clouds analyzed at the center of the domain. Indeed, backward trajectories launched at the time of CALIOP observations (January 28, 10:00 UTC) on the 360 K isentrope, shown on figure 2 (also included in this response), show that : 1) only a limited portion of the air in the cirrus has transited in the South-East part of the domain (this can also be seen in figure 2 of the paper) 2) none of the air parcels went further than 15°South

At last, we also emphasize that nested runs initialised with a larger domain (from 27.5° to 27.5°N and from 158°W to 102°W) also showed this cloud development in the South-East of the domain (see also figure 1 in the response to reviewer 3).

The limited influence of spurious boundary conditions is now mentioned in the Model set-up section, and the nested run is presented in the sensitivity to initial conditions section.

2. **Reviewer** — 2. Ensemble simulations: The simulations are repeated by changing the initial and boundary conditions using ECMWF operational analysis and ERA Interim

data set as well as by switching the microphysical parameterization scheme as "sensitivity tests." Isn't it necessary to conduct ensemble runs to get firm result if there found "the strong dependence to the choice in initial and boundary conditions" (page 31092, lines 20-21)?

Authors — We agree with the reviewer that, if possible, ensemble simulations are a very appropriate tool to characterize the sensitivity to initial conditions. However, it is difficult to conduct such an experiment in our case, for two reasons.

First, the numerical cost of the simulations would be too large, if there were a significant number of ensemble members. Second, there is a major difficulty regarding the preparation of an ensemble: the relevance of ensemble runs depend on the ability of the ensemble members to represent adequately the uncertainty in the region and process of interest. The ensembles developed by operational centers (e.g., ECMWF) are chosen to maximize the variability in the evolution of midlatitude tropospheric perturbations, not in the Tropical Tropopause Layer (TTL). If we started an ensemble of WRF runs from the ECMWF ensemble, there is no guarantee that it would span the right uncertainty in the meteorological fields in the TTL. This choice of ensemble members is really the major caveat. We have used here only a few simulations, carried with the ECMWF operational analysis, ERA interim. We have also carried experiments using NCEP CFSR reanalysis as initial conditions: "Consistently, a simulation with NCEP-CFSR winds and temperature conducted in early stages of this work lead to a cirrus field with significant differences."

To clarify this, we have stated in the text that the sensitivity shown here is more illustrative than a quantitative evaluation. Such sensitivity tests are common practice when carrying out case studies.

3. **Reviewer** — Generalization of the results: The authors conclude that the cirrus clouds have a small effect on radiative budget and do not significantly influence dynamics. Can it be a general conclusion from this particular case study? If not, what is the limitation of this study and what kind of study are needed in the future?

Authors — We want to emphasize that the effect of the clouds in the TTL simulation presented here may seem small, but are actually very significant. In this region of low positive heating rates, the cloud lower the mean LZRH and nearly double the heating rate at 100 hPa, which are very significant effects. This has been stated more clearly in the text.

Regarding the influence on the dynamics, indeed the simulations do not show a strong influence of cirrus radiative heating on circulation. However, we don't think that our case study alone can be used to draw a general conclusion, as it is specific to the environment in which our cloud develop. For instance, the cloud temperature is around 190 K, which is higher than some TTL cirrus, and limits the heating rates. Other real case studies of cirrus clouds in the TTL in different environments would help to settle this issue. We have added a sentence on this in the conclusion.

4. **Reviewer** — Page 31091, line 3: "upwelling trends" might be "upward trends".

Authors — We meant the long-term trends in tropical upwelling. We have changed to "tropical upwelling".

5. **Reviewer** — Page 31092, line 12: "in a region where analyses may present significant errors". If so, is it appropriate to rely on the analysis field for initialization and boundary condition?

Authors — We agree that this may be a problem, but analyses are the only option to initialize such a large domain. The good comparison with cloud observations gives confidence that the initial conditions are sufficiently well represented in the analyses.

6. **Reviewer** — Page 31093, line 21: "bulk microphysics scheme of Thompson et al. (2004)" Some descriptions on the treatment of supersaturation and homogeneous/heterogeneous ice nucleation will help reader to understand.

Authors — More description has been added in section 2.2 following this and referee 1 comment.

7. **Reviewer** — Page 31094, line 13: Correct "the the domain".

Authors — Corrected.

8. **Reviewer** — Page 31097, line 3ff: The color points do not make sense. An alternative will be: set initialization points surrounding the cirrus of interest on the panel for 10:00 UTC on 28 January, and trace the location of those points following the back trajectories until the time of initialization. What we see from the sequence of panels will be the difference in the location of cloud against that of air parcels initially (in a backward sense) surrounded the cloud.

Authors — We have adopted the reviewer's suggestion.

9. **Reviewer** — Page 31098, line 18ff: "there is no clear correlation between w and the cirrus cloud in most of our simulations" The Eulerian vertical velocity is not an appropriate variable to see in situ cloud formation. The cooling rate following the atmospheric motion will be the best. Some more explanation on the difference between "adiabatic upward vertical displacements" and "upward velocities" (lines 21-22) will help interpret the temperature distribution on an isentrope combined with horizontal wind velocity field. In addition, there may be some contribution of the moisture flux from the west near the southern boundary of the simulation region.

Authors — We agree that the important quantity is the temperature change following an air parcel. In the adiabatic limit, it is directly related to the vertical displacement following an air parcel. Regarding the vertical velocity, it gives the instantaneous cooling rates, while the displacement is its integral over some time (since the beginning of the simulation here) and, importantly, following an air parcel. This is now more detailed in the text. The temperature on an isentrope is directly linked to its height, as now shown in figure 4; however, the Lagrangian evolution of temperature cannot be easily predicted from height and wind fields only those fields are not stationary and evolve during the time of the simulation (see fig.2).

10. **Reviewer** — Page 31099, line 3ff: I am skeptical about the usefulness of ΔRH because the ice nucleation depends on the absolute value (not the relative change) of RH .

It will not be consistent with the consideration of supersaturation that does not cause ice nucleation. Another cause of confusion is the reduction of RH after ice nucleation as the cloud formation will be accompanied by the decrease of RH from ~ 1.6 to 1.0.

Authors — We agree with the reviewer, ice nucleation depends on the absolute value of relative humidity (and this is how it is implemented in the microphysics code). The cloud field already illustrates the crossing of the nucleation threshold. Here, our Delta RH aims at evaluating the impact of the vertical motion on (total) relative humidity increase, this increase causing eventually to cross the threshold. The figure hence shows that this change of RH due to the ascents is a good predictor of cloud location. Nonetheless, as noted by the reviewer for the limited area of initially dryer air parcels in the South-East part of the domain, this increase is not always sufficient for ice nucleation.

Regarding the reduction of RH because of water condensation, this was actually taken into account because the RH used to compute Delta RH was not exactly the difference in relative humidity, but the ratio of ice q_{ice} plus water vapour q_{vap} mixing ratio over the ice saturation mixing ratio q_{sat} :

$$\Delta RH = \frac{q_{vap}(\underline{X}(t), t) + q_{ice}(\underline{X}(t), t)}{q_{sat}(\underline{X}(t), t)} - \frac{q_{vap}(0), t_0) + q_{ice}(\underline{X}(t_0), t_0)}{q_{sat}(\underline{X}(t_0), t_0)} \quad (1)$$

Thus, water phase changes will not affect the numerator $q_{vap}(\underline{X}(t), t) + q_{ice}(\underline{X}(t), t)$ along an air parcel trajectory because of the Lagrangian conservation of total water if we neglect sedimentation and diffusion. Only temperature changes will have an impact on the denominator and hence ΔRH . The text was previously misleading and missed to explain that point and this has been corrected.

11. **Reviewer** — Page 31100, line 2: Which part of the symmetric signal is an equatorial Rossby wave? How can it be identified?

Authors — It is difficult to clearly delimit an equatorial Rossby wave in the simulations because of the superposition of many modes and the complex response to the PV intrusion. However, equatorial Rossby modes with PV signature is expected by the PV intrusion.

12. **Reviewer** — Page 31100, line 5: What is Yanai wave? Is it Rossby-gravity wave?

Authors — Yes. This has been clarified in the text.

13. **Reviewer** — Page 31108, lines 4-5: The comparison of the short wave heating between ERA interim and WRF results could be done by estimating the "3 h average that include the sun rise" in WRF simulation.

Authors — We thank the reviewer for this suggestion, that has pointed us out to a mistake in this paragraph. With more investigation, we found that the SW contribution was not at all sufficient to explain the observed difference. Most of the difference actually arises in the long wave. We do not have a clear explanation for this since the temperatures and water vapor are comparable at that altitude. The text has been corrected.

14. **Reviewer** — Page 31112, bottom line: "1000 m in 30 h" What about the corresponding cooling rate in the unit of Kelvin per day?

Authors — -8 K/day, this has been added in the text.

15. *Reviewer* — Page 31113, line 26: "TOA" has first appeared without explanation.

Authors — Corrected.

16. *Reviewer* — Figure 1: The time of observation (top left) and simulation (top right and bottom right) should be identified. Slightly different horizontal/vertical ranges among the top left/right and bottom right panels should be adjusted.

Authors — This has been added. We emphasize that the time of the observation is not exact and only for indication, because it takes about 15 minutes for the satellite to cross the domain.

17. *Reviewer* — Figure 2: I understand the CALIOP observation over the cirrus was at around 10:00 UTC on 28 Jan. 2009. The simulated result of this particular time should not be missed along the time evolution of meteorological fields.

Authors — We have changed the timing of the successive panels following the reviewer's suggestion.

18. *Reviewer* — Figure 3: I don't understand why the distribution at 20:00 is shown rather than 10:00. The left panel, being the same as one of those shown in Figure 2, could be omitted or possibly be changed to illustrate pressure or height of the 360 K isentrope.

Authors — We have followed the advice of the reviewer, and replaced temperature by height.

19. *Reviewer* — Figure 4: Again I don't understand why the distribution at 12:00 is shown rather than 10:00.

Authors — No particular reason, except that 12:00 is a more standard analysis output time. This has been changed for 10:00, but the patterns are similar.

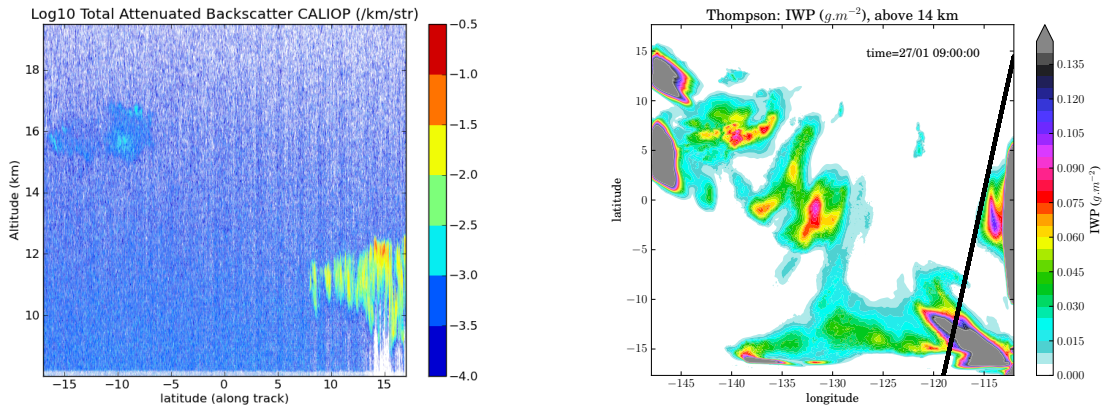


Figure 1: (Left) CALIOP observations over the Eastern Pacific on January 27, 9:00 UTC. (Right) Ice Water Path above 14 km in the simulation on January 27, 09:00 UTC. The black line on the right panel corresponds to CALIPSO track.

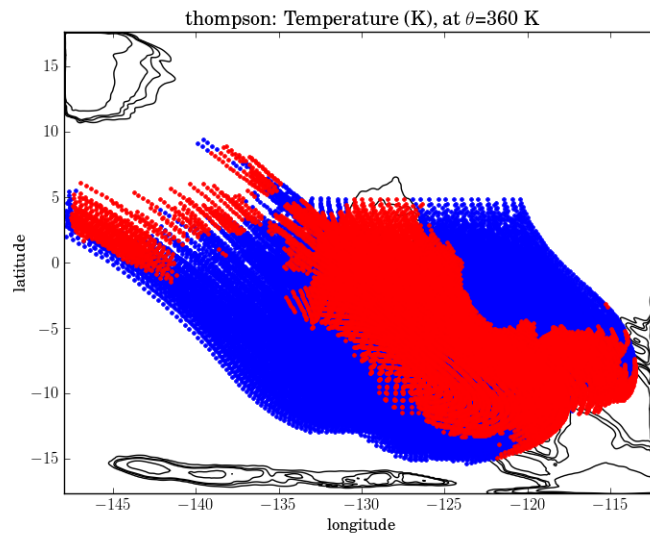


Figure 2: Backward trajectories of parcels initialized at $\theta = 360$ K on January 28, 10:00 UTC. The (backward) initial position position of the parcels span the area between 12.5°S and 5°N and between 134.°W and 120.°W, with a resolution of 0.5°. Trajectory points are colored in red if the air parcel was within a cirrus (IWC ≥ 0.02 ppm), in blue if it was in cloud free air (IWC < 0.02 ppm).

A modelling case study of a large-scale cirrus in the tropical tropopause layer

February 13, 2016

We would like to thank the reviewer for the insightful evaluation of our work. Please find below our point-by-point reply.

1. **Reviewer** — 1) Motivation for this study: In the introduction the authors explain that they focus on this specific cirrus event as it was previously observed and described in Taylor et al. (2011). They should add in the introduction some description of the results of Taylor et al. (2011) so that the readers can understand what were the main results of this study to better justify the focus of this specific cirrus event. There is only one sentence at Line 13 “Taylor et al. (2011) have discussed observations of this cloud” and this sounds rather brief.

Authors — We agree, we have added a paragraph in the introduction with a short description of the results of Taylor et al. (2011) and some motivation for our study.

2. **Reviewer** — 2) Section 2.2 provides a description of the parameterizations used in the WRF simulations. For cloud microphysics, the scheme of Thompson et al. (2004) is used but later in the paper other schemes are used for the sensitivity study (WSM5 and Morrison). Please add these schemes to Section 2.2 and a short description of how they handle ice cloud microphysics. The WRF model has many options for cloud microphysics and some justifications for the use of the scheme of Thompson are missing. Also please add when the simulations are initialized in this section. You mentioned that you performed a 4-day integration but not the initial date. It will help the readers understand that your simulations actually cover the full cloud life cycle.

Authors — Thanks for this comment. We have added the two other schemes in section 2.2, along with the references that were missing. A paragraph has also been added to describe the microphysical assumptions in the Thompson microphysics scheme and justify our choice. We have also added more tests on the sensitivity to ice nucleation, see the text and response to reviewer 1. Also, the time of the start of the simulation is now specified (January 27, 00:00 UTC).

3. **Reviewer** — 3) Comparison with CALIPSO observations: On Figure 1 do you understand why the WRF simulation does not show the extension of the cirrus cloud beyond 5N?

CALIOP shows a rather symmetric cirrus structure that is not seen in the WRF simulation. You later explained that a PV intrusion caused a large-scale uplift and corresponding TTL cooling that is important for the cloud formation. Do you think that extending the northern boundaries of the domain beyond 18N could have helped to improve the representation of the cirrus cloud in WRF?

Authors — Following the reviewer’s comment, we have run an additional simulation using a larger domain, extending up to 28N and a 1-way nested domain run whose boundary conditions are taken from the run with a larger domain. The IWP above 14 km from the 1-way nested run is shown on figure 1 of the present reply. The northern limit of the cloud is not much changed. Also, we want to emphasize that, if along CALIPSO path the cloud does not extend beyond 5N in the reference simulation, a few degrees to the East the cloud field almost reaches 10N (see figure 1 of the paper). So this disagreement along the track does not necessarily mean that the actual and simulated clouds are so dissimilar regarding their northern extension. We have added a sentence mentioning this point in the paper.

4. **Reviewer** — 4) You mentioned a large difference of 3K between simulated and analyzed temperature fields in section 2.3. Since TTL water vapor and temperature are important for in situ cirrus cloud formation and thus for this case event, have you compared the model representation of TTL water vapor and temperature with observations? e.g. water vapor from MLS and temperature from COSMIC since there are very few radiosondes for this region.

Authors — We thank the reviewer for this comment, that allows us to discuss a difficult point. Actually, we have carried a comparison with MLS water vapour measurements, which are almost synchronous and colocated with CALIOP measurements. The comparison did not prove satisfactory: while values at 100 hPa were much comparable, the observations below 100 hPa (around 121-147 hPa) were systematically dry biased compared to the simulations. The disagreement is of the same order as discrepancies between ECMWF analyses and MLS reported by Jiang et al. (2015) (up to 5 ppmv for our simulation without applying the averaging kernels). This discrepancy could be a concern because 121-150 hPa is actually the main level of cirrus formation in the simulation. We do not think it is a major concern for our simulation, for the following reason: comparison of MLS and frost point measurement have shown a mean bias of 3 ppmv at 147 hPa in the tropics (after applying the averaging kernels) and differences have been reported to reach more than 2 ppmv at 121 hPa and 6 ppmv at 147 hPa, according to a comparison with Frost Point Hygrometer measurement on which the MLS averaging kernels were applied (Hurst and Coauthors, 2015). The sharp water vapour vertical gradients in this region, due to the cirrus, seem to make MLS measurements less reliable at that altitude. This points out the difficulty linked to the lack of in situ measurements in the tropical tropopause layer for real case simulations.

Regarding COSMIC observations, the ECMWF analyses assimilate them so we regarded the analyses as representative of those observations.

5. **Reviewer** — 5) “We do not look for any further validation of the microphysical properties of the cloud either (such as in cloud supersaturation and ice crystal number), because of the absence of observational data for this case.” Even though you do not have observational data for

this specific case, you could use results from other observational studies of cirrus clouds in the Eastern Pacific (e.g. Davis et al. [2010] or Jensen et al. [2013]) to compare qualitatively the properties (ice crystal number concentration, particle size, supersaturation) of this cirrus event. It could help to assess whether this specific cirrus event is representative of cirrus formation in the Eastern Pacific.

Authors — Following this reviewer’s comment, and the comment of reviewer 1, we have added some comparison of our simulation and in situ observations in Table 2 of the revised paper and in the text; see also answer to reviewer 1.

6. **Reviewer** — 6) Lagrangian trajectories and air parcels on Figure 2. Could you add some descriptions release time and location of the air parcels? On Figure 2, does one point correspond to the center of mass of different points?

Authors — We have changed this figure and the displayed trajectories following reviewer 2’s comments. The trajectories now displayed on the figure are released at 360 K on January 28, 10:00, at the horizontal position shown on the corresponding panel of figure 2; they are individual trajectories. This has been specified in the paper.

7. **Reviewer** — 7) For the radiative heating rates shown on Figure 8, in addition to the the comparison with ERAi radiative heating rates, you could also compare the WRF estimates with Figure 3 of Corti et al. (2006). Of course, the comparison would be only qualitative since you have heating rates from a 4-day simulation while Corti et al. used 6 years of balloon sonde measurements of temperature, ozone, and water vapor profiles from the SHADOZ network and cloud observations to compute mean full sky radiative heating rates in the tropics.

Authors — We have added their estimation on figure 7 of the paper. Corti et al.’s calculations predict a substantially stronger effect of local clouds but, as stressed by the reviewer, the comparison can only be qualitative as we examine here a specific cloud field over a specific region. We discuss the curves in the text.

References

- Hurst, D. and Coauthors: Water Vapor Measurement Biases in the TTL: MLS vs Frost Point Hygrometers, in: CT3LS meeting, Boulder, Colorado, URL <http://esrl.noaa.gov/csd/events/CT3LS/presentations/wed-posters-4-hurst.pdf>, 2015.
- Jiang, J. H., Su, H., Zhai, C., Wu, L., Minschwaner, K., Molod, A. M., and Tompkins, A. M.: An assessment of upper troposphere and lower stratosphere water vapor in MERRA, MERRA2, and ECMWF reanalyses using Aura MLS observations, Journal of Geophysical Research: Atmospheres, 120, 11,468–11,485, doi:10.1002/2015JD023752, URL <http://dx.doi.org/10.1002/2015JD023752>, 2015.

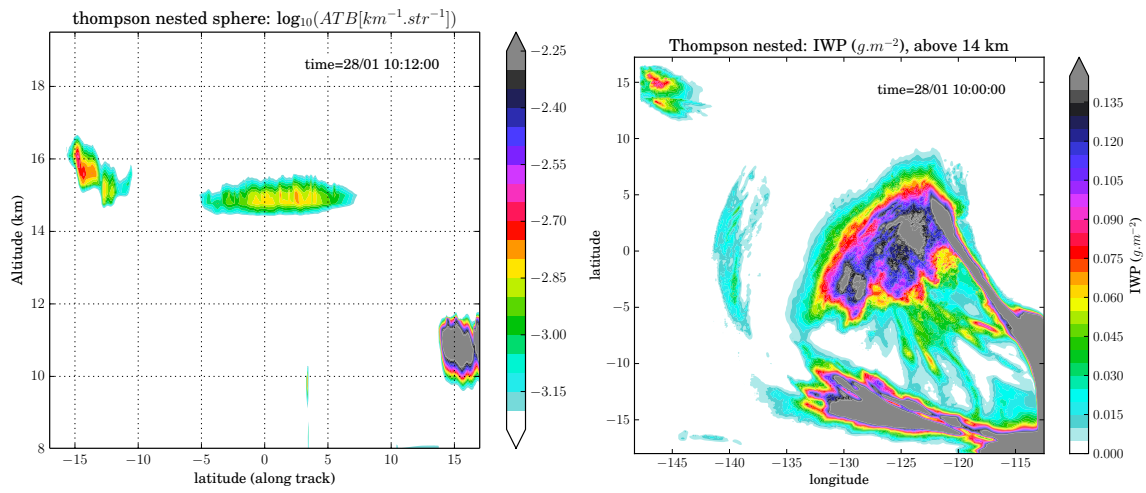


Figure 1: (Left) Simulated ATB along CALIOP track for the nested model run, on January 28 at 10:00 UTC. (Right) Ice water path above 14 km on January 28 at 10:00 UTC.

Manuscript prepared for Atmos. Chem. Phys. Discuss.
with version 2014/09/16 7.15 Copernicus papers of the \LaTeX class copernicus.cls.
Date: 13 February 2016

A modelling case study of a large-scale cirrus in the tropical tropopause layer

Aurélien Podglajen¹, Riwal Plougonven¹, Albert Hertzog¹, and Bernard Legras¹

¹Laboratoire de Météorologie Dynamique (LMD), CNRS-UMR8539, Institut Pierre Simon Laplace, École Normale Supérieure, École Polytechnique, Université Pierre et Marie Curie, Paris, France

Correspondence to: Aurélien Podglajen, aurelien.podglajen@lmd.polytechnique.fr

Abstract

We use the Weather Research and Forecast (WRF) model to simulate a large-scale tropical tropopause layer (TTL) cirrus, in order to understand the formation and life cycle of the cloud. This cirrus event has been previously described through satellite observations by Taylor et al. (2011). Comparisons of the simulated and observed cirrus show a fair agreement, and validate the reference simulation regarding cloud extension, location and life time. The validated simulation is used to understand the causes of cloud formation. It is shown that several cirrus clouds successively form in the region due to adiabatic cooling and large-scale uplift rather than from ~~ice lofting from~~ convective anvils. The structure of the uplift is tied to the equatorial response (equatorial wave excitation) to a midlatitude potential vorticity (PV) intrusion ~~structures the uplift~~.

Sensitivity tests are then performed to assess the relative importance of the choice of the microphysics parametrisation and of the initial and boundary conditions. The initial dynamical conditions (wind and temperature) essentially control the horizontal location and area of the cloud. On the other hand, the choice of the microphysics scheme influences the ice water content and the cloud vertical position.

Last, the fair agreement with the observations allows to estimate the cloud impact in the TTL in the simulations. The cirrus clouds have a small but not negligible impact on the radiative budget of the local TTL. However, for this particular case, the cloud radiative heating does not significantly influence the simulated dynamics. ~~The~~ This result is due to (1) the lifetime of air parcels in the cloud system, which is too short to significantly influence the dynamics, and (2) the fact that induced vertical motions would be comparable to or smaller than the typical mesoscale motions present. Finally, the simulation also provides an estimate of the vertical redistribution of water by the cloud and the results emphasize the importance in our case of both re and dehydration in the vicinity of the cirrus.

1 Introduction

Cirrus are the most frequent type of clouds, covering about 30 to 50 % of the Earth surface (Stubenrauch et al., 2010), and they have non negligible impact on the global radiative energy budget (Lohmann and Roeckner, 1995). From remote-sensing observations, they seem nearly ubiquitous in the tropical tropopause layer (~~TTL, Fueglistaler et al., 2009~~) (TTL) (Wang et al., 1996; Fueglistaler et al., 2009). Radiative transfer calculations suggest that they strongly influence the heat balance of the TTL, potentially controlling its temperature and contributing to ~~upwelling trends~~ tropical upwelling (Corti et al., 2005). Cirrus are furthermore believed to control the dehydration of air masses and the amount of water vapour that enters the stratosphere (Jensen et al., 1996).

Despite the remarkable attention TTL cirrus have received for the last 20 years, the microphysical processes controlling their formation are still largely debated. More precisely, the respective importance of homogenous and heterogeneous nucleation remains unclear, although in situ observations suggest that both are active in the TTL (Jensen et al., 2013; Cziczo et al., 2013). Contrary to the microphysics, the dynamics leading to cirrus seems somehow better understood. The clouds result either from ice detrainment from convective towers or from in situ formation in supersaturated regions created by large to mesoscale uplifts (Wang and Dessler, 2012). Nevertheless, the role of different waves with different scales in cirrus processes is still discussed, and their impacts still require quantification (Kim and Alexander, 2015).

Many processes regarding TTL cirrus have been studied using a Lagrangian framework (parcel or single column models, Jensen and Pfister (2004)) or with idealised mesoscale simulation (e.g., Jensen et al., 2011; Dinh et al., 2012). There have been relatively few studies conducting meso to large scale modelling of real-case TTL cirrus. Different reasons may contribute to this: the fact that the typical spatial scale of TTL cirrus can go down to a few meters in the vertical, the many unknowns in the microphysics, and the uncertainty regarding how detailed the microphysics modelling needs to be (bin or bulk). However, despite these important limitations, simulations using a mesoscale model of tropical cirrus

have nonetheless been carried out, but in a climatological perspective, i.e. using a moderate resolution and several months of simulations (Wu et al., 2012; Evan et al., 2013). Now, mesoscale simulations can also be used for case studies of individual clouds, to address issues such as the dynamical causes of cloud formation. Such case studies will first contribute to evaluating the realism of the macrophysical characteristics of the simulated cirrus (location, altitude, timing, extent). If these characteristics are successfully modeled, the model simulation may serve to explore the cirrus evolution and its impact. Recently, Muhlbauer et al. (2014) used case studies with a mesoscale (cloud resolving) model to explore the sensitivity of different types of cirrus to modifications of the microphysical parameters and to modifications of the initial conditions, but the mesoscale model tool has mainly been used to study midlatitude cirrus (e.g. Muhlbauer et al., 2015). In this paper, we use the Weather Research and Forecast ARW (Advanced Research WRF or WRF ARW, Skamarock et al. (2008)) model to conduct ~~such~~ a real-case study of an in situ formed TTL cirrus cloud, ~~with focus on the large-scale characteristics~~. The case studied corresponds to a cloud having a very large spatial extent and occurring over the Eastern Pacific, ~~i. e. in~~ . This cloud event was pointed out by Taylor et al. (2011) , who described it using satellite observations. In particular, Taylor et al. (2011) have shown that the cloud occurred within a large-scale low temperature anomaly, which was itself probably related to a midlatitude Potential Vorticity intrusion. The probable large-scale in-situ formation of this cloud makes it suitable for a mesoscale model case study, because one can hope that the analyses used to force the model contain the necessary dynamical component to drive the cirrus formation, although the Eastern Pacific is a region where analyses may present significant errors due to the sparsity of observations (Podglajen et al., 2014). ~~Taylor et al. (2011) have discussed observations~~ Finally, the choice of this cloud for the study is also motivated by the possibility to investigate the potential influence of dynamics-radiation interaction, that may have played a role in the cloud evolution for this case (Taylor et al., 2011).

The paper is organised as follows. In section 2, the model setup and an overview of the cirrus event in the simulations are described. We show that despite uncertainties and crude assumptions in its microphysical parametrisation, the model is able to reproduce

the main characteristics of the observed cloud structure. In section 3, we explain that this good agreement between observed and modelled clouds is tied to the well-represented large-scale dynamics. Section 4 illustrates **diverse** several sensitivity studies and the strong dependence to the choice in initial and boundary conditions. Finally, section 5 discusses the modelled impact of the cloud in the tropical tropopause layer.

2 Model and observations

2.1 Case description

The study focuses on a cirrus cloud forming in the Tropical Eastern Pacific in late January 2009. This case was highlighted as remarkable for its very large horizontal extent by Taylor et al. (2011), who analyzed it in satellite observations. In observations from the Cloud-Aerosol LiDAR with Orthogonal Polarization (CALIOP, Winker et al., 2007), one can identify the large region covered by the cirrus through its intensified backscatter (Fig. 1, top left panel, similar to Figure 1 of Taylor et al. (2011)). In particular, the cloud seems to extend almost continuously over 3000 km along track, at an altitude between 15 and 16 km. In addition to this considerable spatial extent, Taylor et al. (2011) furthermore showed that high clouds were seen on CALIOP tracks during several days (27-29 January) and suggested that they could be portions of the same extensive cirrus. The cloud would then extend several thousand kilometers in the zonal direction as well, and last a few days.

Regarding the atmospheric flow in the Tropical Eastern Pacific region, where the cloud forms, climatological Westerlies dominate at upper-tropospheric levels, as part of the Walker circulation. However, they can be strongly modulated at synoptic times scales. This is the case at the time of our simulation, as we will see in Sect. 3.

2.2 Model description and setup

To simulate the cirrus event, we use the Weather Research and Forecast (WRF) mesoscale model (Skamarock et al., 2008). The relevant elements of our reference setup are described

in the following, while the different sensitivity tests that were carried out will be the subject of Sect. 4.

Regarding physical parametrisations, microphysical processes are treated with the bulk microphysics scheme of Thompson et al. (2004), which has two moments for the ice class. Short and long wave radiative heating rates are calculated using the Rapid Radiative Transfer Model G (RRTMG, Iacono et al., 2008). RRTMG is fully coupled to the Thompson microphysics, and accounts for the radiative effect of cloud particles through their mass and effective radius. In the radiative calculations, the values of well-mixed greenhouse gas concentrations and of the ozone mixing ratio are taken from the Community Atmosphere Model with Chemistry (CAM-chem) outputs, with monthly and latitudinal variations (see WRF Users' guide). Finally, the initial and lateral boundary conditions come from the ECMWF operational analysis, which at that time had 91 vertical levels and a T1279 spectral resolution (corresponding to a horizontal resolution of about 0.125 degrees).

About domain specifications, our spatial domain extends from 18° South to 18° North and from 148° West to 112° West (i.e., about 4000*4000 km), and the nominal horizontal resolution is 10 km (i.e. 400*400 points). The domain was chosen to surround the cloud seen in CALIOP observations on figure 1. It is large enough so that the development of the cirrus clouds at its center is not much affected by the boundary conditions, according to trajectory analysis. In the vertical, there are 120 levels extending up to 8 hPa, with the last 7 km taken as a sponge layer to avoid spurious wave reflection. The resulting vertical resolution around 15 km is approximately 300 m. The model is initialised on July 27, at 00 UTC. Although we performed a 4-day integration for the reference simulation, the paper is focused on the shorter period 27-29 July. One reason is that this time period includes the observations along Calipso track shown in Fig. 1. Another reason is that in longer simulations, at the altitudes considered (14-17 km), most of the air that was initially inside ~~of the the domain got~~ the domain has been advected out of it within two days or less, thus preventing the analysis with tracers initialised in the initial condition (see Sect. 3 and 5). In addition to this, the first twelve hours of the simulation are regarded as spin-up, and not shown. This

is conservative : deep convection is very limited in our simulations, so little adjustment to latent heat release is expected, resulting in an effective spin-up time of only a few hours.

In the reference simulation, microphysical processes are treated with the bulk microphysics scheme of Thompson (Thompson et al., 2004, 2008; Thompson and Eidhammer, 2014), which has two moments for the ice class. The ice number concentration is assumed to follow an exponential distribution with respect to the diameter. The mass-diameter relationship adopted is $m(D) = \rho_i \frac{\pi}{6} D^3$ with $\rho_i = 890 \text{ kg}\cdot\text{m}^{-3}$ standing for ice density, i.e. the ice crystals are assumed to be spherical. With two moments for ice, differential sedimentation occurs in the scheme with different mass weighted and number weighted terminal fallspeeds. The scheme allows for ice supersaturation and includes homogeneous nucleation (Koop et al., 2000) and an empirical treatment that could be considered as heterogeneous nucleation. Here, the heterogeneous ice nuclei are activated once a supersaturation threshold $S_{nuc} = 8\%$ is reached, and their number N_{IN} follows the observations of Cooper (1986) above 233 K, and are saturated to their value at 233 K (i.e. 1500 crystals per liter) below that. These values of N_{IN} and S_{nuc} may seem unlikely for heterogeneous ice nuclei concentrations and properties at 15-16 km in the TTL, although no direct measurements in this region are available for comparison to our knowledge. We emphasize that, if one can interpret this procedure as heterogeneous nucleation, it can also be better thought as an empirical parametrisation of the combined effect of heterogeneous and homogeneous nucleation triggered by resolved and unresolved perturbations inside the 10 km*10 km*300 m grid box. This explains the rather low supersaturation for ice formation, that compensates for the fact that the box mean supersaturation is below the local maxima encountered within the grid box. To address the sensitivity to the nucleation-related parameters (N_{IN} and S_{nuc}), we have performed sensitivity tests that are described in Sect. 4 together with the sensitivity to the microphysics scheme. Moreover, we have also used the microphysical schemes of Morrison et al. (2005) (Morrison) and Hong et al. (2004) (WSM5), which handle nucleation at cold temperature in a similar way as Thompson scheme. Those experiments are also presented in Sect. 4. Our choice of the default Thompson scheme as reference within the many WRF microphysics scheme is a compromise between keeping acceptable

computational costs and describing potentially important processes such as differential sedimentation; it is also motivated by the good comparison with observations obtained in this configuration, presented below.

Short and long wave radiative heating rates are calculated using the Rapid Radiative Transfer Model G (RRTMG, Iacono et al., 2008). RRTMG is fully coupled to the Thompson microphysics, and accounts for the radiative effect of cloud particles through their mass and effective radius. In the radiative calculations, the values of well-mixed greenhouse gas concentrations and of the ozone mixing ratio are taken from the Community Atmosphere Model with Chemistry (CAM-chem) outputs, with monthly and latitudinal variations (see WRF Users' guide). Finally, the initial and lateral boundary conditions come from the ECMWF operational analysis, which at that time had 91 vertical levels and a T1279 spectral resolution (corresponding to a horizontal resolution of about 0.125 degrees).

2.3 Model validation against CALIPSO observations

In order to compare WRF outputs with CALIOP observations, we use the LiDAR simulator from the Cloud Feedback Model Intercomparison Project Observation Simulator Package (COSP, see Chepfer et al. (2008) for a description). Light scattering by ice particles is a complicated problem, and in theory depends on the size distribution, shape and orientation of ice crystals on top of their concentration. In the COSP LiDAR simulator, only the dependences of the LiDAR signal to ice concentration and ice crystal effective radius are retained. Those two are calculated consistently between the different microphysical parametrisations used and the LiDAR simulator.

For the comparison, we will mainly use the observed and simulated total attenuated backscatter (ATB) at 532 nm without any normalization. The ATB is an almost direct measurement, and the absence of normalization is appropriate as long as we are interested in one specific and limited altitude range. Figure 1 shows the along-track profiles of the ATB observed by CALIOP (top left) and simulated by WRF-COSP (top right) for the reference case on 28 January 2009. Despite the crude microphysical treatment of ice nucleation in the reference Thompson scheme, there is an overall good agreement between observed and

simulated cirrus cloud location and extension (quantitative evaluation will be used in Sect. 4 to compare different choices for the simulations). [The northern extension of the cloud field appears underestimated along CALIPSO track, but the simulation does show an extension beyond 5°N to the East of the track \(see Fig. 1\).](#)

5 This agreement qualitatively validates the simulation of the general dynamics which led to cloud formation. However, the model visually seems to underestimate the backscatter by a factor of about 2. Possible reasons **for this disagreement** are the uncertainties associated with measurement noise (typically about 35-50% of the measured ATB for our cloud) and approximations and uncertainties in the calculated backscatter from WRF outputs. Shape
10 assumptions is one source of such uncertainties. Here, the choice of the ATB for comparison implies that the hypothesis about ice crystal shapes are made in the COSP LiDAR simulator and not in the retrieval. Hence, we do not rely on the LiDAR ratio chosen in the CALIOP retrieval algorithm, on the contrary to what would have happened if we had used CALIOP's extinction coefficients for example (Mioche et al., 2010). This allows us to evaluate the sensitivity to shape assumptions directly by varying parameters in COSP. Among
15 the choices available, we have tested for differences between spherical and non-spherical prolate shapes. The results for this experiment are illustrated on Fig. 1 (top right and bottom right panels). The strong difference in amplitude seen between the two panels agrees with results stressed for instance by Cirisan et al. (2014), who showed that changing the assumed aspect ratio of prolate spheroids by 20% could modify the backscatter by a factor of 2. For our simulation, the best agreement in the signal amplitude is achieved assuming spherical crystals, which agrees with [the shape assumption in the microphysics scheme and with](#) observations of the shape of small TTL ice crystals (McFarquhar et al., 2000).
20 [At last, beside shape assumptions, the type of ice crystal size distribution assumed also affects the simulated ATB; however, we did not test the sensitivity to this parameter to keep consistency with the microphysical parametrisation \(exponential distribution\).](#) In light of the strong unknowns in the measurements and in the comparison procedure, the agreement found between the top left and right panels in Fig. 1 is very encouraging.

In addition to the "comparison related" uncertainties mentioned above, the disagreement between the observed and simulated backscatter intensities may also be due to an underestimation of the ice water content (IWC). A number of factors could then be involved: inappropriate microphysics, too much diffusion of water vapour in the model, underestimation of the water vapour content in the initialisation, or overestimation of the temperature. In fact, it is likely that several of those factors are at play and partly compensate, e.g. underestimation of both water vapour and supersaturation. In the absence of more constraining data, we do not attempt here any tuning of the initial conditions but we will provide some discussion on the sensitivity to those in Sect. 4. ~~We do not look for any further validation of the microphysical properties of the cloud either (such as in cloud supersaturation and ice crystal number), because of the~~ Due to the absence of ~~observational data for this case.~~ in situ observational data for this case, it is impossible precisely evaluate the simulated microphysics. However, as shown in Table 2, we note that the simulated cloud microphysical properties are comparable to in situ observations by Lawson et al. (2008) and within the range of other observations from Krämer et al. (2009); Davis et al. (2010); Jensen et al. (2013).

Finally, one should add that the simulated and analyzed temperature fields show significant local departures from one another, up to 3 K at 16 km, 36 hours after initialisation, though no systematic bias is noted. Those differences typically correspond to meso-scale structures of $\sim 1,000$ km horizontal extent, yet they have small amplitudes (< 0.5 K) in the region with significant ice water content. With these differences in absolute temperature, it may be rather surprising that the simulated cloud is so similar to observations. This arises because of the strong constraint provided by the large-scale dynamics leading to the cloud formation. This is the subject of Sect. 3, but first an overview of the cirrus evolution in the simulation is provided in the next subsection.

2.4 Simulated cirrus evolution

Figure 2 shows the evolution of the temperature and cirrus field in the simulation, at the potential temperature level $\theta = 360$ K. On those maps, we see that the correlation between

the cloud field and low temperature anomalies, as observed by Taylor et al. (2011), is reproduced in the WRF simulation. As expected due to the dependence of microphysical processes on relative humidity, which itself depends on temperature, the cloud development closely follows the evolution of low temperatures in the simulation.

5 The color points on the figure illustrate some individual air parcels positions initialised on 28/01, 10:00 at $\theta = 360$ K and the horizontal position shown on the panel corresponding to this time on figure 2. The displacement of those air parcels comes from backward and forward (kinematic) Lagrangian trajectories calculated with the wind field in the simulation. Due to diabatic heating, the potential temperature level of those air parcels obviously
10 changes during the time of the simulation. However, the trajectory calculations show that this change is limited to less than 1 K during the simulation, which is consistent with the value of diabatic heating rates. Hence the representation of those points on the isentrope $\theta = 360$ K does not introduce any qualitative bias.

One point that those trajectories show conclusion from those trajectories is that, although
15 the flow has a stagnation point and weak velocities at the center of the domain (see the evolution of the red point position between 27/01 at 18:00 and 29/01 at 00:00 blue and black point positions), air parcels nonetheless experience significant variations in temperature, partly due to the Westward displacement of the cold temperature anomaly. Moreover, aside for from air parcels near the stagnation point region, significant horizontal displacements are
20 found (on of the order of a thousand km per day). Different clouds are always present in the simulation but, due to the temperature variability along the trajectory (which is linked to different meso-scale perturbations), they do not follow air parcels and this limits the in-cloud residence-time for each cloud. This problem of in-cloud residence-time in the simulation will be addressed in more details detail in Sect. 5.2.

25 One last important property of this cloud field is that, despite its "patchy" feature, different clouds appear in the same regions, which suggest some large-scale forcing of the cloud. In the following section 3, the causes of cloud formation in the simulation will be examined more precisely.

3 Dynamical features leading to cloud formation

3.1 Cause of ice cloud formation

Cirrus clouds in the TTL can either form in situ through the cooling of ascending air masses, or they can result from ice lofting from convective clouds (Fueglistaler et al., 2009). For our case, Taylor et al. (2011) argued that the latter was unlikely due to the horizontal extent of the cloud. Furthermore, there was no evidence of deep convection taking place in the region of interest at that time in CALIPSO observations. To support their assertion, we have introduced passive boundary layer tracers at the beginning of the simulation (27 January 00:00:00 UTC). None of them had reached the cirrus altitude (>14 km) at the end of the simulation.

Hence in situ formation prevails here, and it must happen through the cooling of ascending air masses. Using GPS radio-occultation temperature measurements, Taylor et al. (2011) showed that the synoptic situation in the cirrus region was associated with a cold temperature anomaly in the TTL. The strong link of the cirrus clouds with low temperature anomalies in the simulation (can be seen in Fig. 2) is once more shown in Fig. 3 (left panel), where the cirrus, highlighted by the contours of the ice water content, tend to be present in the coldest regions. One naturally thinks of cold temperature anomalies as associated with strong constant upward vertical velocities, because of the cooling associated with adiabatic expansion which relates air parcels (Lagrangian) cooling rates $\frac{DT}{Dt}$ and w through :

$$\left(\frac{DT}{Dt}\right)_{adiabatic} = -\frac{g}{C_p}w$$

where $g = 9.81 \text{ m/s}^2$ is gravitational acceleration and $C_p = 1004. \text{ J/kg/K}$ is the thermic capacity of dry air at constant pressure. Yet, there is no clear correlation between w and the cirrus cloud in most of our simulations (not shown). While this may seem puzzling at first, it simply reflects that the simulated clouds formed in wave-induced negative temperature anomalies , in phase with adiabatic ΔT , which are related to upward vertical displacements

ments ~~rather than~~ ξ , i.e. time-integrated Lagrangian vertical velocity, rather than directly with upward velocities.

~~To~~ Indeed, in the dry adiabatic limit,

$$\Delta T = -\frac{g}{C_p}\xi = -\frac{g}{C_p}\int_X w(\underline{X}(t), t)dt$$

5 where \int_X is the integral following $\underline{X}(t)$ the air parcel position. Because of the horizontal velocity, uplift cannot be estimated directly with instantaneous w . A more appropriate quantity is the height of an isentropic surface, which is shown for instance for January 28, 10:00 UTC on Fig. 3, left panel. There is a good correlation of this height with the cirrus and temperature; however, the height of the isentrope is not computed following an air parcel and does not enable to quantify the uplift created by the dynamics in the simulation.

10 To quantify this more precisely, we have computed Lagrangian trajectories in the WRF simulation. This also allows to evaluate the upward displacement in the more natural altitude coordinate, which is that of CALIOP observations. The deduced uplift, calculated since the start of the simulation, is shown in Fig. 4, left panel. Part of the figure is intentionally
 15 left blank, because the corresponding air was not in the domain at the initial time. The cirrus location is clearly associated with ~~the strongest vertical uplift~~ strong vertical uplifts, and the northern limit of the cloud corresponds to a reversal of the sign of the vertical displacement, which becomes negative in the northern part of the domain. To further show that the simulated relative humidity is actually controlled by the vertical displacement field
 20 and not directly by the initial conditions, we have also computed a ΔRH , which is defined as ~~the difference between initial and current relative humidity along an air parcel trajectory:~~

$$\Delta RH = \underline{RH}_{now} - RH_{ini} \frac{q_{vap}(\underline{X}(t), t) + q_{ice}(\underline{X}(t), t)}{q_{sat}(\underline{X}(t), t)} - \frac{q_{vap}(o), t_0 + q_{ice}(\underline{X}(t_0), t_0)}{q_{sat}(\underline{X}(t_0), t_0)} \quad (1)$$

This quantity where $X(t)$, $X(t_0)$ indicate that we follow a Lagrangian trajectory, q_{sat} is the mass saturation mixing ratio with respect to ice, and q_{vap} and q_{ice} are the ice and vapor mass mixing ratios. Neglecting sedimentation and diffusion, the numerator of the two terms is the same (Lagrangian conservation of the total water). Hence, this quantity, which is shown in the right panel of Fig. 4. ~~Its strong correlation~~, evolves Lagrangianly because of the change of the denominator $q_{sat}(X(t), t)$, which is due to the vertical displacement and the associated adiabatic temperature change. It allows to distinguish the contribution of the simulation internal dynamics in driving a Relative Humidity increase from the initial conditions. The strong correlation of ΔRH with the cirrus location (shown by the black contours) confirms that in this case study the simulated cirrus forms because upward the vertical displacement caused an increase in the relative humidity, and not because the relative humidity was already high enough in the initial conditions. Still, initial relative humidity, if too dry, can impact the cloud location because the ice formation threshold is not reached, as seen in the South-East part of the domain. However, figure 4 shows that the dynamically induced vertical displacement exerts a strong control over the cloud structure.

3.2 Large scale dynamics

A large scale uplift thus explains the formation of the clouds, but the question of the cause of this uplift remains. Taylor et al. (2011) pointed out that the cold temperature anomaly was most likely related to dynamical features originating in the extratropics. In particular, they showed a map of potential vorticity from NCEP reanalysis at 200 hPa (see their figure 9), illustrating midlatitude intrusions of high PV anomalies extending in the region where the cirrus form. A comparable figure for our simulation is displayed in Fig. 3, right panel, which shows the potential vorticity at $\theta = 360$ K. A clear northern hemisphere PV intrusion can be identified on this figure and the large-scale dynamics in the simulation is likely strongly affected by this structure.

This kind of influence from the midlatitudes is common in the Eastern Pacific upper troposphere (Vaugh and Polvani, 2000), where the average Westerly winds associated with the Walker circulation enable inter-hemispheric interactions. Intruding in tropical regions, the

midlatitude signals are expected to excite equatorial modes (Kiladis and Feldstein, 1994). We examined this using fields from the ERA interim. Figure 5 shows a Hovmoeller diagram of the (left) symmetric and (right) antisymmetric components of the 125 hPa temperature between 15°S and 15°N, with zonal wind contours added on the left panel and meridional wind contours on the right. The symmetric signal shows quasi-stationarity features, which could be the signature of an equatorial Rossby wave. On the contrary, the antisymmetric signal clearly shows westward phase propagation, and antisymmetric temperature are in phase with the meridional wind component. This moving pattern is consistent with the signature of a Yanai [\(or mixed Rossby-gravity\)](#) wave, and explains the antisymmetric structure in which the cirrus forms that was seen on Fig. 3, left panel. The Yanai wave interpretation is also consistent with the quadrature phase relationship between symmetric zonal anomalies of the potential vorticity and antisymmetric temperature anomalies (Fig. 3, both panels).

The onset of this "Yanai wave" style perturbation in the domain and its vertical structure are depicted more clearly in Fig. 6, which shows a vertical Hovmoeller diagram of antisymmetric temperature and symmetric meridional wind at 130°W. Meridional wind and antisymmetric temperature exhibit a downward phase propagation in the cirrus altitudes (in agreement with expectations for upward-propagating Yanai wave packets). It is worth noting that the "Yanai wave" perturbation seen here differs from the free-travelling Yanai waves observed in the equatorial lower stratosphere. Its period is longer (~10 days versus 4-5 typically in the lower stratosphere) and its phase speed lower. This is probably due to several factors such as the low frequency of the midlatitude interaction that excites the wave-like response, Doppler shift, the interaction with the equatorial Rossby wave pattern, and the complicated sheared wind structure (see Wang and Xie, 1996) over the Eastern Pacific at that time. Such long period (6-10 days in our case) westward propagating Yanai waves seem common in the Westerly duct and have been observed in [operational](#) analyses by Randel (1992).

The combination of the symmetric and antisymmetric temperature signals creates negative temperature anomalies in the South-East part of the domain, which is also the region of strongest vertical displacements. Hence, the large scale dynamics during the simulation is

dominated by a midlatitude PV intrusion that excites Yanai (and probably Rossby) equatorial wave modes, which are themselves responsible for the vertical displacements in the upper troposphere. These wave-induced vertical displacements are the necessary component to increase the supersaturation and cause the cirrus formation.

5 Although the main structure of the cirrus is dominated by the large-scale waves, other waves contributing to the vertical displacement might also have an impact on the temperature anomaly and may influence cirrus formation. However, for a given trajectory the spectrum of vertical displacements emphasizes more the contribution of motions with slower intrinsic frequencies. In the present case, where large-scale motions with significant vertical
10 displacements are present, the contribution from smaller scale motions (inertia gravity waves) to the vertical displacement needed to produce the cirrus clouds seems secondary to understand the cloud pattern.

4 Sensitivity of the simulated cirrus cloud

The large-scale uplift is thus a first-order element needed to produce the cirrus field. Accurate cirrus cloud simulations involve this and other components, ranging from a good
15 description of the water vapour field to meso-scale gravity waves, as well as appropriate microphysics and radiative parametrisations. The sensitivity of the simulated cirrus to some of those components will be presented in the following subsections once the methodology for comparing the simulations is introduced. A summary of all simulations presented in this
20 section can be found in Table 1.

4.1 Comparison methodology

Different characteristics of the cloud field should be compared between simulations and observations. Along a CALIOP track, cloud location and extension ("cloud fraction") are important properties to be evaluated on top of the averaged returned backscatter. Their
25 evaluation depends on subjectively chosen thresholds for the cloud limits, but can nevertheless provide more objective insights into the differences than a visual comparison. Cloud

location and amplitude will be used to determine how the different simulations compare with the observations.

On top of the comparison with the observations, it is also necessary to conduct comparisons of the simulations with one another, to capture the spatial structure better than only with the along-track view provided by CALIOP. We have used maps of the simulated Ice Water Path (IWP, vertically integrated ice water content) above 14.5 km for this purpose. The (dis)similarity of the obtained maps is evaluated using standard correlations and the SAL metrics, which have been introduced by Wernli et al. (2008) and previously used to evaluate cirrus simulations by Kienast-Sjögren et al. (2015). The SAL consists in 3 components: Structure (S), Amplitude (A) and Location (L). A perfect match between the fields (exactly similar) corresponds to the score 0 for Structure, Amplitude and Location. More precisely, the Structure and Amplitude components take values between -2 and 2, while the Location component is bounded by 0 and 2. The structure, S, compares the shape of the two cloud fields (many small clouds versus one huge cloud). Positive values indicate a more dispersed cloud field than the reference. The Amplitude A compares the average IWP, positive values corresponding to an overestimation relatively to the reference. This A component takes no consideration on the spatial structure. The last component, L, summarizes the error in the spatial location of the field (the location of its center of mass).

The comparisons of the different fields with observations are presented in Table 4, which reports the differences in the vertical and horizontal location of the centroid of the returned backscatter between observation and simulations, as well as the differences in the amplitude of the returned backscatter (calculated as the A component of the SAL). The maps of the ice water path (IWP) above 14.5 km are shown in Fig. 7 and the corresponding correlations with the reference setup and SAL metrics are reported in Table 5.

4.2 Sensitivity to initial conditions

Previous studies have shown TTL cirrus modelling to be strongly sensitive to initial conditions, for instance the initial water vapour content ([\(?\) \(Dinh et al., 2016\)](#)). To assess this sensitivity, we have carried out different sets of simulations varying the initial and the boundary

conditions (see Table 1). With two different microphysics schemes (Morrison and Thompson), we have performed simulations with ERA interim and the ECMWF operational analysis initial and boundary conditions. The reference simulation uses the operational analysis for initialisation and boundaries. We have also performed a ~~simulation-nested model run with~~ a coarser horizontal resolution (30 km) simulation launched on January 25 over a larger domain (extending from 27.5° to 27.5°N and from 158°W to 102°W) from the operational analysis. It served as initialisation for another simulation in our reference domain at 10 km resolution. This experiment can also be viewed as a sensitivity test to domain size. At last, we have conducted an additional simulation initialised with the operational analysis ~~field~~ but with the fields, but with a homogeneous 20 % increase in the initial water vapour content ~~increased by 20~~. This bias is in the range of observed disagreements between the ECMWF operational analysis and in situ observations (Kunz et al., 2014). We emphasize that all those experiments are mainly illustrative and may not span the uncertainty linked to initial and boundary conditions.

Table 4 shows that the reference simulation offers the best agreement with the observations in amplitude, and a close centroid location. The center of mass of the attenuated backscatter is about 300 m (less than one model level) lower in this simulation than in observations. All simulations put the cloud centroid too much to the south, which is linked to an along-track underestimation of the northward extension of the cloud compared to observations. All simulations also underestimate the intensity of the ATB, except the one with increased initial water vapour. The change in the initial condition mainly results in a change in the location of the cloud, ~~which is moved further southward~~. While in the nested simulation the cloud is comparable in mean location to the reference, and does not extend as poleward as in the observations, in the simulation initialised with the ERA interim, the cloud is moved further southward (Table 4).

This effect of southward displacement of the cloud in the simulation with ERA interim is also shown in the IWP maps in Fig. 7. The cloud pattern is changed in the same way for the two microphysics schemes presented: the slightly different dynamics and water vapour in ERA interim simulations result in a cloud structure moved in the southern part of the domain.

In terms of SAL metrics (Table 5), depending on the scheme, the amplitude in the ERA interim simulations can be increased (Thompson) or decreased (Morrison) compared to those that use the operational analysis. These contrasted responses are due to the different behaviors of the two schemes in the context of a competition between a moister initial condition in cirrus formation regions in the ERA interim simulations and stronger uplifts in the northern part of the domain for simulations with the operational analysis. On the other hand, for the two schemes, the correlations with the reference are significantly decreased (below 0.65) when the ERA interim is used for initialisation. This mainly comes from a change in the location term, and the simulation that uses ERAi with Thompson is the one that shows the highest (about 0.14) location parameter for the SAL. Finally, regarding the structure component S of the SAL, initial and boundary conditions are the most sensitive factors.

We must emphasize that the sensitivity to the initial conditions refers in fact to both the initial dynamics of the simulation (e.g. initial distribution of the potential vorticity) and the initial relative humidity. To isolate one from the other, we have also performed a simulation with the ECMWF operational analysis initial and boundary winds and temperature, but with the ERA interim water vapour field (not shown). Our water vapour does not strongly affect the dynamics because of the limited occurrence of convection in the domain. The simulated cirrus is then very similar to the one obtained with the operational analysis fields in terms of location and structure; it shows higher IWC, consistently with the discussion above (moister ERA interim). This experiment highlights again that, due to the importance of the uplifts and the strong vertical gradient of water vapour content, the cloud structure is controlled more by the dynamically induced vertical displacement than by the initial distribution of humidity. Consistently, a simulation with NCEP-CFSR winds and temperature conducted in early stages of this work lead to a cirrus field with significant differences.

The specific effect of changing the initial relative humidity is also shown ~~in-*yb*~~ the simulation with ~~a-homogeneous~~ 20% increase ~~in initial water vapour~~ of the water content. It has little effect on the horizontal characteristics of the cloud field (see the correlation, location or structure in Table 5). However, its effect is not limited to increasing the IWC but it also

tends to lower the cloud altitudes (see Table 4) by bringing regions below the cloud in the reference simulation to supersaturation and hence prolongating vertically the fall streaks generated by the initial cloud.

4.3 Sensitivity Some sensitivities to the microphysical scheme in WRF microphysics

5 As stated in the Introduction, there has been much debate regarding microphysical pathways of cirrus cloud formation (Spichtinger and Krämer, 2013). Recent measurements and modelling studies suggest that strong variability may get to scales as small as a few meters (~~e.g., Jensen et al., 2013; Murphy, 2014; ?~~) (e.g., Jensen et al., 2013; Murphy, 2014; Dinh et al., 2014) unreachable in our model setup. Hence we do not attempt to delve in the details of the microphysics, ~~but simply~~. We evaluate the sensitivity to some microphysical assumptions by two simple approaches. First, we just take advantage of the schemes available in WRF to test how sensitive the simulated cirrus clouds are to changes within a range of standard parametrisations. Then, inside the Thompson scheme, we modify the ad hoc parameters for nucleation at low temperature : number of Ice nuclei N_{IN} and supersaturation threshold for ice nucleation S_{nuc} .

4.3.1 Sensitivity to the microphysical scheme in WRF

We performed tests with one single-moment ~~parametrisation, the scheme~~ (WSM5) and two double-moment schemes, the Thompson and Morrison schemes. ~~All~~ In this study, all those schemes use the same very empirical approaches of the nucleation at low temperature as the Thompson scheme, but their different numerical treatments of sedimentation and growth lead to some sensitivity.

On Fig. 7, one can compare the IWP produced by the Thompson and Morrison schemes for the two initial and boundary conditions tested. The two schemes produce similar (correlated, see Table 5 for correlation with the reference) cloud fields but their intensities differ. The Morrison simulation tends to have higher ice water content than the Thompson simulation. The difference is mainly due to the integrated effect of sedimentation (it almost van-

ishes if sedimentation is suppressed), the Morrison scheme having a less efficient sedimentation ([more details on the different treatments of sedimentation can be found in appendix A](#)). This lower downward flux of ice in the simulations with the Morrison scheme [also](#) explains that the cloud is higher in those compared to CALIPSO observations (see Table 4).
5 Vertical profiles confirm this effect of higher IWC in the Morrison scheme (not shown).

In terms of SAL metrics, Table 5 shows that the main component affected by the different choice in microphysics is the amplitude, i.e. the mean value of the Ice Water Path. However, the correlations are higher, and the structure and location components are more similar between the different schemes than between different initial and boundary conditions. Also,
10 it appears clearly in this table that the different choices made in the two-moments schemes make them as dissimilar from one another as from the WSM5 one-moment scheme.

4.3.2 [Sensitivity to some bulk microphysics parameters : number of "Ice Nuclei" and supersaturation threshold for nucleation](#)

[In order to explore further the sensitivity to microphysical parameters, we have also run sensitivity simulations with different supersaturation thresholds \$S_{DUC}\$ and "Ice Nuclei Number" \$N_{IN}\$. Because of our coarse resolution relatively to what is needed to resolve microphysical processes, we emphasize that the chosen supersaturation threshold is not meant to fit experimental data of homogeneous or heterogeneous nucleation. Rather, it has to account for the fact that, within one model grid box, temperature and/or water vapor fluctuations will cause the relative humidity to rise above the actual \(experimentally measured\) threshold for the particles that are present, while the grid box average remains below this value \(Kärcher and Burkhardt, 2008\) . However, the chosen value is ad hoc and the sensitivity to it should be assessed. Besides the default value of 8%, we have tested values for threshold supersaturation of 20%, 30% and 45%. Regarding the Ice Nuclei number concentration \$N_{IN}\$, as 1500 #/L may appear strong as a default value for the grid-box-mean effect of nucleation, we have tested reducing it to 150 #/L.](#)

15
20
25

[Figure 8 shows maps of the Ice Water path above 15 km for two simulations with the Thompson scheme keeping the same \$N_{IN} = 1500\$ and varying the supersaturation threshold](#)

($S_{nuc} = 0.2$ and 0.45); these figures can also be compared to the reference simulation in the top left panel of Fig. 7. They show that, over some range of S_{nuc} , the large-scale cloud field is only weakly dependent on S_{nuc} : between $S_{nuc} = 0.08$ and $S_{nuc} = 0.2$, there is only a change in the absolute IWP value, which is diminished due to more grid point not experiencing nucleation and keeping ice-free. This ice mass decrease can also be seen in Table 5 in the Amplitude component of the SAL. Despite the amplitude difference, the general cloud pattern is itself very similar between the simulations with $S_{nuc} = 0.08$ and $S_{nuc} = 0.2$, as confirmed by the strong correlation with the reference (Table 5). When a critical value for the threshold is exceeded, however, nucleation does not happen in some parts of the cloud and the pattern is much affected; this is the case for the experiment with $S_{nuc} = 0.45$. Changing N_{IN} between $N_{IN} = 150\#/L$ and $N_{IN} = 1500\#/L$ had only minor impact on the large-scale properties of the simulated cloud field (Table 5), which may result from an increase in the portion of the cloud experiencing nucleation.

The overall bulk microphysical properties of the clouds are relatively weakly affected by the change, as reported in Table 3. We emphasize that this is much different from parcel model results, because the area covered by the clouds change from a simulation to the other and we select only cloudy air (i.e. with IWC bigger than $5.e-8$ kg/kg) to compute the statistics. N_{IN} has a limited impact. S_{nuc} variation create much more substantial variability. However, this stays within the variability observed in TTL cirrus clouds, which scans several order of magnitude (Jensen et al., 2013).

Overall, the result of those experiments show that there is robustness of the simulated cirrus large-scale and microphysical properties for a range of values of the parameters which lies within reasonable values. This is reassuring given the uncertainty of those parameters in our simulation framework.

4.4 Sensitivity to radiation

Previous [real-case](#) studies have shown that interaction with radiation could have a strong influence in the [high](#) cloud field evolution for midlatitude cases (Gu et al., 2011). [Idealised](#) simulations suggest that this may also be the case for TTL cirrus, at least under specific

environmental conditions (Dinh et al., 2010; Jensen et al., 2011). In Fig. 7, the IWP from simulations with (top) and without (bottom) cloud radiative effect included ~~are displayed in Fig. 7 is displayed~~. There is little difference between the two simulations, and this is confirmed by the very high correlation (0.97) and the small amplitude component of the SAL metrics (Table 5). On this time scale (36 hours after the beginning of the simulation), it seems that there is little impact on the cirrus field. We will discuss possible reasons for this negligible impact of the radiation in our case in Sect. 5.

4.5 Resolution

It should be noted that the results we present are for a specific resolution, which is probably too low to adequately simulate some of the processes at stake. Nevertheless, increasing the vertical resolution by a factor of 2 ~~the vertical resolution or or the horizontal one~~ by a factor 2.5 ~~the horizontal one~~ created little quantitative changes to the simulated cirrus cloud field. This illustrates that in our setup and with our typical resolution (a few kilometers in the horizontal, a few hundred meters in the vertical), sensitivity to resolution has not yet appeared. This is also linked to the relative lack of convection in the domain, and to the first-order influence of the forcing provided by the large scale-dynamics.

4.6 Summary of sensitivities

For our cirrus case, the combination of the correlations and of the amplitude component of the SAL metrics in Table 5 allows some ranking of sensitivities. The dynamics is of first order, even so after 36 hours of simulation the impact of microphysics and initial water vapour are also important. The choices of the parametrisation of microphysical processes and of the initial water content do not affect the cloud field like dynamics does: they mainly influence the cloud "amplitude" and vertical position. The 'dry' dynamical initial and boundary conditions (winds and temperature), and the different dynamics and water vapour field they create through different advection, are more important to determine the cloud structure and location, and have the strongest impact on correlations. The relatively moderate role of de-

tails in the water vapour field is reassuring because this quantity is poorly known at fine scale in the TTL. It explains why we obtain a good agreement with the observations without any tuning of the initial water vapour. Finally, Table 5 shows that, in our case, the cloud radiative effect results in much less sensitivity than the other factors, because of the relatively low heating rates.

5 Discussion

5.1 Evaluation of the cirrus radiative impact in the TTL

Cirrus clouds are believed to strongly influence the radiative budget of the TTL by increasing the radiative heating rates. In this region of low positive heating rates, even a small contribution from cirrus could significantly enhance the transport efficiency and strongly lower the transit time of ascending air parcels from the TTL to the stratosphere (Corti et al., 2006). Based on the satisfactory agreement with observations ([see Sect. 2.3](#)), our simulations allow us to provide a reliable estimate of the radiative impact of this specific cloud in the tropical tropopause layer. To evaluate this, we have performed simulations with the cloud radiative heating artificially turned off in the RRTM scheme. The resulting profiles of radiative heating rates averaged over the domain are shown in Fig. 9. For comparison, the same profiles in the ECMWF ERA interim reanalysis [and the zonal annual mean profiles calculated by Corti et al. \(2006\)](#) are also displayed for clear and all sky radiative heating rates ~~at the same time~~. Note that the heating rates profiles displayed here are in actual temperature tendency and not in potential temperature tendency.

In the upper TTL ([above 90 hPa](#)), the WRF simulation seems to underestimate the heating rates compared to the ERA interim. ~~This apparent disagreement is a short wave effect~~ [They are in better agreement with Corti et al. \(2006\)](#). ~~This disagreement mainly comes from long wave differences, and might be~~ due to different ~~time averaging between the simulation and the reanalysis~~. ~~The ERA interim heating rates are indeed 3 hours averages that include the sun rise, whereas the WRF heating rates are instantaneous nighttime~~

values. ozone mixing ratios but was not investigated further as it is above the main levels of interest.

In the lower part of the TTL (below 90 hPa) ~~where the short wave impact is negligible~~, there is a fair agreement between the heating rates in the ERA interim and in the WRF simulation, which use different versions of the same RRTM scheme, as well as with those estimated by Corti et al. (2006). However, the difference between clear and all sky heating rates in the reanalysis is very limited, while there is a significant enhancement of the heating in the simulations even after averaging over the whole domain. From the difference between the WRF simulations with and without cloud radiative heating included, we estimate the domain-averaged cloud radiative effect to be of the order of 0.1 K.day^{-1} . This contribution moves the Level of Zero Radiative Heating by about 10 hPa (i.e. about 500 m) below its clear sky value. This is ~~comparable to the estimate a factor of about 2-3 smaller than the estimates~~ by Corti et al. (2006) for the whole tropics. ~~This shown on the figure, which is probably due to geographic heterogeneities of the cloud field in the tropics with much colder and denser clouds in the boreal winter Western Pacific. We also emphasize that this~~ is a domain average, but instantaneous values in the cloud can be much more substantial, reaching up to $1.5\text{-}2 \text{ K.day}^{-1}$. This is comparable to estimates of the order $1\text{-}3 \text{ K.day}^{-1}$ observed by Bucholtz et al. (2010), but higher than values in subvisible cirrus reported by Davis et al. (2010). This figure also stresses that a poor representation of the cirrus in the reanalysis probably leads to an underestimation of the additional heating rate induced by the cloud.

5.2 Absence of a cloud scale (re)circulation, and observed cloud duration

Recent studies (e.g. Dinh et al., 2012; Jensen et al., 2011) have examined the potentially important role of cloud-induced radiative heating to drive cloud-scale circulation in TTL cirrus. Among other results, the presence of magnitude of wind shear was found to be an important factor ~~that could prevent affecting the buildup of~~ cloud-scale circulations (Jensen et al., 2011).

We examined the dynamical impact of cloud radiative heating for our simulated cirrus, by comparing the simulations with and without cloud radiative heating. Only minor differences were found for the cirrus evolution (see Table 5). Although the situation was *a priori* ideal for a cloud-scale circulation to build (cloud above the ocean, with little convection below), several factors can explain its absence in our simulations. First, our radiative heating rates are too low to generate such a circulation, although they are comparable to the lower values reported in the literature for modelling studies (e.g., Dinh et al., 2012). Then, our vertical resolution of 300 m may be too coarse to resolve this recirculation in the cloud and its surrounding. However, increasing the vertical resolution by a factor of 2 did not produce any significant change. Going back to physical reasons, Jensen et al. (2011) suggested that, in most cirrus, the Lagrangian temperature variability along an air parcel trajectory was such that it would limit the cloud lifetime, which would then be too short for a radiatively-induced circulation to build. We estimated the in-cloud residence time using Lagrangian trajectories: forward and backward trajectories were calculated from initial positions within the cloud (IWC higher than $1\text{e-}10\text{ kg.kg}^{-1}$), spaced every 1 degree in latitude and longitude and every 500 m in the vertical. The resulting probability density functions for the in-cloud residence time of air parcels is displayed in Fig. 10. The typical lifetime is less than 10 hours, which is probably too short for a radiative circulation to build and have significant impact on the cloud evolution. This result for our cirrus is in agreement with what was found for different TTL cirrus by Jensen et al. (2011) .

On top of this cloud-lifetime limitation, there is another reason explaining the absence or at least the very limited impact of a cloud scale (re)circulation in our test case: that is the amplitude of this circulation. It will obviously depend on the background stability and heating efficiency but idealised studies (Dinh et al., 2010, 2012) suggest that, in the most favourable cases and in a two-dimensional setting, those circulations will not exceed a few m.s^{-1} in the horizontal and a few cm.s^{-1} on the vertical. These velocities and the associated shears are at most comparable to and often smaller than the ambient velocities and shears (e.g. the amplitude of cirrus induced wind shear in idealised simulations reaches at most $5\text{ m.s}^{-1}.\text{km}^{-1}$ (Dinh et al., 2012)). In the vertical, typical large-scale to mesoscale motions

which generate cirrus formation and cause cirrus dissipation can be of the order of a few $\text{cm}\cdot\text{s}^{-1}$. Hence, in cases such as ours, the radiatively induced vertical motion are not strong enough to come out relative to other motions present.

Finally, the set of simulations we have performed suggests that even if TTL cirrus appear to last several days, as suggested by Taylor et al. (2011), this can rather correspond to a succession of distinct clouds forming in a region of persistent favorable conditions. As for orographic ~~clouds (e.g. lenticular)~~ lenticular clouds that can persist above mountains, the cloudy air parcels in the TTL cirrus clouds in our region are different through the cloud presence time. Cloud radiative heating seems not to play an important impact on the dynamics in our specific case and it is probably not required to explain the long-duration of the cloud.

5.3 Cloud induced vertical redistribution of water vapour

One major issue associated with TTL cirrus is water vapour redistribution, which produces the irreversible dehydration (freeze-drying) experienced by air parcels that transit through the TTL before entering the stratosphere. Dinh et al. (2014) have used idealised simulations to illustrate that different scenarios for water vapour redistribution could arise depending on the cloud environment, with layers of dehydration and rehydration. Similar estimates are not possible in our modelling configuration, because we do not use periodic boundary conditions. In our limited area simulations, there are air and water mass fluxes leaving and entering the domain through its boundaries. To provide an estimate of the water redistribution due to the cloud field nevertheless, we have introduced a passive water tracer in the simulations. The water tracer is advected and diffused using the same numerics as the moisture field (positive definite advection) but it is not subject to any physical, or more precisely microphysical source nor sink. We evaluate the integrated impact of those microphysical sources and sinks, i.e. the vertical redistribution of water by the cloud, through the difference between the unaffected (advected only) water vapour field and the fully microphysically interactive water vapour.

Figure 11 shows the profile of the difference between microphysically passive and active water. To avoid being affected by the boundary conditions, we have introduced a second

passive tracer for the "inner domain", i.e. the part of the domain whose air was inside the domain at the initial time. We have computed the difference only over this area, which depends on the altitude range considered due to wind vertical shear. Hence, the passive water is affected by exchange with air coming from the boundaries only in a limited "diffusion" range. This is less true for the active water due to the sheared vertical structure of our "inner domain" and the sedimentation. That is why we can only provide a rough estimate of the vertical redistribution of water in the simulation. Here, three colored curves are shown for three different simulations. The green curve corresponds to a "No sedimentation" test in which we artificially suppressed sedimentation for temperatures below 220 K (the cirrus regime); the consistence of our calculation is validated by the closeness of this curve to a 0 ppm change in total water above 14 km. The blue curve shows the evaluation of redistribution for the Thompson scheme; with this scheme the cirrus dehydrates by about 0.5 ppm above 15.5 km and rehydrates below this altitude (by about 0.5 ppm). Finally, the red curve corresponds to a "Maximum Dehydration" simulation in which the microphysics in the cirrus regime has been replaced by a simple hypothesis of removal of all water above 100% relative humidity with respect to ice (there is no ice for this simulation). Comparison of the red and blue curves illustrates the overestimation of dehydration and the missed rehydration made with this hypothesis, which is close to what has been used for Lagrangian trajectory modelling of stratospheric water vapour (e.g. Fueglistaler and Haynes, 2005).

We emphasize that the calculated redistributions are very dependent on the microphysical scheme and microphysical assumptions. Nevertheless, our simulations show the importance of vertical redistribution of water associated with dehydration, which is known but may have been previously overlooked. Indeed, the dominant paradigm in calculations on dehydration along Lagrangian trajectories (e.g., Liu et al., 2010) is that the water vapour source is exclusively from below and that the last dehydration (i.e. coldest point along the trajectory) determines the water vapour concentration of air entering the stratosphere. This neglects the possibility of rehydration by sedimenting crystals, which constitutes another source of water vapour. Moreover, because of horizontal and vertical heterogeneities in the

dehydration patterns, hydration by sedimenting ice crystals can modulate these patterns and the intensity of dehydration. In particular, Fueglistaler et al. (2014) recently illustrated that the stratospheric water response to a temperature drop associated with an increase in tropical upwelling would not follow the Clausius-Clapeyron scaling. By reducing the residence time of air in the TTL and thus the probability of air parcels to experience the coldest TTL temperatures (bounded in some geographic regions), the vertical velocity increase mitigates the temperature drop effect. If the TTL residence time indeed contributes to control dehydration, it is probable that rehydration (from in situ cirrus or anvil ice) does not fully cancel out. In any case, limited (by microphysical processes) dehydration or rehydration (by sedimenting ice crystals) certainly contribute to influence the amount of water vapour and ice in the TTL.

6 Conclusions

We have performed a case-study of large-scale cirrus clouds in the Eastern Pacific using a mesoscale model, the Weather Research and Forecast model (Skamarock et al., 2008). These simulations complement the previous study of the same case by Taylor et al. (2011), which was based on observations, and test the ability of the WRF model to reproduce cirrus clouds in the tropical tropopause layer. The simulations compare well with CALIPSO observations, suggesting that the dynamical processes leading to the cirrus formation are well captured by the model. They confirm that the cirrus forms in-situ due to large-scale uplift associated with the response to a mid-latitude potential vorticity intrusion. At the equator, this PV intrusion excites an equatorial wave response, mainly Yanai ([mixed Rossby-gravity](#)) and equatorial Rossby modes, that are modulated by faster inertia-gravity waves. The vertical displacements associated with this atmospheric flow are of the order of 1000 m in 30 hours ([equivalent to a mean cooling rate of -8 K/day](#)) and generate an increase in the relative humidity which is responsible for the formation of the cirrus clouds. Although the cloud forms in regions of relatively weak winds and has a large horizontal extent (several hun-

dreds to more than a thousand of kilometers), trajectory calculations show that air parcels transit through the cirrus on timescales of about half a day.

This study highlights the importance of dynamical forcing on TTL cirrus formation: large-scale uplift associated with low-frequency perturbations provide the necessary drop in temperature for the cloud to form. The presence of the cirrus is robust between the two re-analyses systems tested (the ECMWF ERA interim reanalysis and operational analysis), because they both resolve the PV intrusion which is a large-scale feature. The simulated clouds are sensitive to the dynamics, but also to the microphysical scheme and to the distribution of water vapour, in different ways: differences in the dynamics affect the location, amplitude and structure of a cloud field, while the microphysics and water vapour mainly influence the intensity of the cloud and its vertical position and extent. The strong dependence to the dynamics, i.e. to the initial and boundary conditions provided by analyses, implies a serious difficulty for real-case simulations, because analyses notoriously have deficiencies in the description of winds in the TTL (Podglajen et al., 2014). In contrast to the sensitivity to dynamics and microphysics, the simulated cloud showed little sensitivity to radiative effects: in particular, the simulations showed no sensitivity of the cirrus field to radiation. More precisely, the simulations showed no evidence of a circulation on the scale of the cloud driven by radiative effects, likely reasons being that the cloud residence times are short (half a day) and that the radiatively induced heating rates are rather weak. [As this result might be tied to the specific environment in which the cloud develops \(e.g. its relatively warm temperature of about 190 K\), more real-case simulations are needed in the future to evaluate the impact of cloud radiative heating on the dynamics in different environments.](#)

Finally, the simulations illustrate the importance of dehydration and its associated rehydration in the TTL. This is important to understand the entry of stratospheric water vapour, but also the water budget of the TTL itself. We emphasize that the latter is also of importance and has non negligible impacts for the [TOA-top of the atmosphere \(TOA\) radiative fluxes](#) (Riese et al., 2012).

Appendix A: Ice sedimentation in Thompson and Morrison schemes

In the version of the Thompson scheme used in this work, the sedimentation fall speed of a single ice crystal depends on its diameter D under the form:

$$v(D) = \left(\frac{\rho_0}{\rho} \right)^{0.5} \alpha D^\beta \quad (\text{A1})$$

5 The coefficients are $\alpha = 1847.5$ and $\beta = 1$; they have been chosen to produce a smooth transition with the snow category (Thompson et al., 2008) . In the Morrison scheme, ice sedimentation follows :

$$v(D) = \left(\frac{\rho_0}{\rho} \right)^{0.35} a D^b \quad (\text{A2})$$

10 where $a = 700$. and $b = 1$.; at the considered altitudes, there is a factor 2 to 3 between the fall speeds in the Morrison and Thompson's schemes, which explains the higher IWC observed in the Thompson scheme.

Acknowledgements. The authors are grateful to Sophie Bastin, Marjolaine Chiriaco and H el ene Chepfer for help with the COSP. We thank Martina Kr amer, Jens-Uwe Groo , Joan Alexander, Eric Jensen and Bill Randel for helpful discussions, and Pasquale Sellitto for his comments on the manuscript. A.P. and R.P. received support from Ecole Polytechnique's Chaire pour le D veloppement Durable (DDX). R.P., A.H., B.L. and A.P. acknowledge support from ANR project StraDyVariUS (Stratospheric Dynamics and Variability, ANR-13-BS06-0011-01) and from E-U project StratoClim. The support of CNES through 'Strat ole' project is also acknowledged.

References

20 Bucholtz, A., Hlavka, D. L., McGill, M. J., Schmidt, K. S., Pilewskie, P., Davis, S. M., Reid, E. A., and Walker, A. L.: Directly measured heating rates of a tropical subvisible cirrus cloud, J. Geophys. Res., 115, D00J09, doi:10.1029/2009JD013128, 2010.

- Chepfer, H., Bony, S., Winker, D., Chiriaco, M., Dufresne, J.-L., and Sèze, G.: Use of CALIPSO lidar observations to evaluate the cloudiness simulated by a climate model, *Geophysical Research Letters*, 35, n/a–n/a, doi:10.1029/2008GL034207, <http://dx.doi.org/10.1029/2008GL034207>, 2008.
- 5 Cirisan, A., Luo, B. P., Engel, I., Wienhold, F. G., Sprenger, M., Krieger, U. K., Weers, U., Rommens, G., Levrat, G., Jeannet, P., Ruffieux, D., Philipona, R., Calpini, B., Spichtinger, P., and Peter, T.: Balloon-borne match measurements of midlatitude cirrus clouds, *Atmospheric Chemistry and Physics*, 14, 7341–7365, doi:10.5194/acp-14-7341-2014, <http://www.atmos-chem-phys.net/14/7341/2014/>, 2014.
- 10 Corti, T., Luo, B. P., Peter, T., Vömel, H., and Fu, Q.: Mean radiative energy balance and vertical mass fluxes in the equatorial upper troposphere and lower stratosphere, *Geophys. Res. Lett.*, 32, L06 802, doi:10.1029/2004GL021889, 2005.
- Corti, T., Luo, B. P., Fu, Q., Vömel, H., and Peter, T.: The impact of cirrus clouds on tropical troposphere-to-stratosphere transport, *Atmos. Chem. Phys.*, 6, 2539–2547, doi:10.5194/acp-6-2539-2006, 2006.
- 15 Cziczo, D. J., Froyd, K. D., Hoose, C., Jensen, E. J., Diao, M., Zondlo, M. A., Smith, J. B., Twohy, C. H., and Murphy, D. M.: Clarifying the dominant sources and mechanisms of cirrus cloud formation., *Science*, 340, 1320–1324, doi:10.1126/science.1234145, 2013.
- Davis, S., Hlavka, D., Jensen, E., Rosenlof, K., Yang, Q., Schmidt, S., Borrmann, S., Frey, W., Lawson, P., Voemel, H., and Bui, T. P.: In situ and lidar observations of tropopause subvisible cirrus clouds during TC4, *J. Geophys. Res.*, 115, D00J17, doi:10.1029/2009JD013093, 2010.
- 20 Dinh, T., Durran, D. R., and Ackerman, T.: Maintenance of tropical tropopause layer cirrus, *J. Geophys. Res.*, 115, D02 104, doi:10.1029/2009JD012735, 2010.
- Dinh, T., Durran, D. R., and Ackerman, T.: Cirrus and water vapor transport in the tropical tropopause layer – Part 1: A specific case modeling study, *Atmos. Chem. Phys.*, 12, 9799–9815, doi:10.5194/acp-12-9799-2012, 2012.
- 25 Dinh, T., Fueglistaler, S., Durran, D., and Ackerman, T.: Cirrus and water vapour transport in the tropical tropopause layer – Part 2: Roles of ice nucleation and sedimentation, cloud dynamics, and moisture conditions, *Atmos. Chem. Phys.*, 14, 12 225–12 236, doi:10.5194/acp-14-12225-2014, 2014.
- 30 Dinh, T., Podglajen, A., Hertzog, A., Legras, B., and Plougonven, R.: Effect of gravity wave temperature fluctuations on homogeneous ice nucleation in the tropical tropopause layer, *Atmospheric Chemistry and Physics*, 16, 35–46, doi:10.5194/acp-16-35-2016, <http://www.atmos-chem-phys.net/16/35/2016/>, 2016.

- 5 Evan, S., Rosenlof, K. H., Dudhia, J., Hassler, B., and Davis, S. M.: The reWater Vapor Measurement Biases in the Tropical Tropopause Layer: Aura Microwave Limb Sounder vs Frost Point Hygrometers presentation of the TTL in a tropical channel version of the WRF model, *Journal of Geophysical Research: Atmospheres*, 118, 2835–2848, doi:10.1002/jgrd.50288, <http://dx.doi.org/10.1002/jgrd.50288>, 2013.
- Fueglistaler, S. and Haynes, P. H.: Control of interannual and longer-term variability of stratospheric water vapor, *J. Geophys. Res.*, 110, D24 108, doi:10.1029/2005JD006019, 2005.
- Fueglistaler, S., Dessler, A. E., Dunkerton, T. J., Folkins, I., Fu, Q., and Mote, P. W.: Tropical tropopause layer, *Rev. Geophys.*, 47, RG1004, doi:10.1029/2008RG000267, 2009.
- 10 Fueglistaler, S., Liu, Y. S., Flannaghan, T. J., Ploeger, F., and Haynes, P. H.: Departure from Clausius-Clapeyron scaling of water entering the stratosphere in response to changes in tropical upwelling, *Journal of Geophysical Research: Atmospheres*, 119, 1962–1972, doi:10.1002/2013JD020772, <http://dx.doi.org/10.1002/2013JD020772>, 2014.
- Gu, Y., Liou, K. N., Ou, S. C., and Fovell, R.: Cirrus cloud simulations using WRF with improved radiation parameterization and increased vertical resolution, *Journal of Geophysical Research: Atmospheres*, 116, n/a–n/a, doi:10.1029/2010JD014574, <http://dx.doi.org/10.1029/2010JD014574>, 2011.
- Hong, S.-Y., Dudhia, J., and Chen, S.-H.: A Revised Approach to Ice Microphysical Processes for the Bulk Parameterization of Clouds and Precipitation, *Mon. Wea. Rev.*, 132, 103–120, doi:10.1175/1520-0493(2004)132<0103:ARATIM>2.0.CO;2, [http://dx.doi.org/10.1175/1520-0493\(2004\)132<0103:ARATIM>2.0.CO;2](http://dx.doi.org/10.1175/1520-0493(2004)132<0103:ARATIM>2.0.CO;2), 2004.
- 20 Iacono, M. J., Delamere, J. S., Mlawer, E. J., Shephard, M. W., Clough, S. A., and Collins, W. D.: Radiative forcing by long-lived greenhouse gases: Calculations with the AER radiative transfer models, *Journal of Geophysical Research: Atmospheres*, 113, n/a–n/a, doi:10.1029/2008JD009944, <http://dx.doi.org/10.1029/2008JD009944>, 2008.
- Jensen, E. and Pfister, L.: Transport and freeze-drying in the tropical tropopause layer, *J. Geophys. Res.*, 109, D02 207, doi:10.1029/2003JD004022, 2004.
- Jensen, E. J., Toon, O. B., Pfister, L., and Selkirk, H. B.: Dehydration of the upper troposphere and lower stratosphere by subvisible cirrus clouds near the tropical tropopause, *Geophys. Res. Lett.*, 23, 825–828, doi:10.1029/96GL00722, 1996.
- 30 Jensen, E. J., Pfister, L., and Toon, O. B.: Impact of radiative heating, wind shear, temperature variability, and microphysical processes on the structure and evolution of thin cirrus in the tropical tropopause layer, *J. Geophys. Res.*, 116, doi:10.1029/2010JD015417, 2011.

- Jensen, E. J., Diskin, G., Lawson, R. P., Lance, S., Bui, T. P., Hlavka, D., McGill, M., Pfister, L., Toon, O. B., and Gao, R.: Ice nucleation and dehydration in the Tropical Tropopause Layer, *Proc. Nat. Acad. Sci.*, 110, 2041–2046, doi:10.1073/pnas.1217104110, 2013.
- 5 Kienast-Sjögren, E., Miltenberger, A. K., Luo, B. P., and Peter, T.: Sensitivities of Lagrangian modeling of mid-latitude cirrus clouds to trajectory data quality, *Atmospheric Chemistry and Physics Discussions*, 15, 7535–7584, doi:10.5194/acpd-15-7535-2015, <http://www.atmos-chem-phys-discuss.net/15/7535/2015/>, 2015.
- Kiladis, G. and Feldstein, S.: Rossby wave propagation into the tropics in two GFDL general circulation models, *Climate Dynamics*, 9, 245–252, 1994.
- 10 Kim, J.-E. and Alexander, M. J.: Direct impacts of waves on tropical cold point tropopause temperature, *Geophysical Research Letters*, 42, 1584–1592, doi:10.1002/2014GL062737, <http://dx.doi.org/10.1002/2014GL062737>, 2015.
- Koop, T., Luo, B., Tsias, A., and Peter, T.: Water activity as the determinant for homogeneous ice nucleation in aqueous solutions, *Nature*, 406, 611–614, doi:10.1038/35020537, 2000.
- 15 Krämer, M., Schiller, C., Afchine, A., Bauer, R., Gensch, I., Mangold, A., Schlicht, S., Spelten, N., Sitnikov, N., Borrmann, S., de Reus, M., and Spichtinger, P.: Ice supersaturations and cirrus cloud crystal numbers, *Atmos. Chem. Phys.*, 9, 3505–3522, doi:10.5194/acp-9-3505-2009, 2009.
- Kunz, A., Spelten, N., Konopka, P., Müller, R., Forbes, R. M., and Wernli, H.: Comparison of Fast In situ Stratospheric Hygrometer (FISH) measurements of water vapor in the upper troposphere and lower stratosphere (UTLS) with ECMWF (re)analysis data, *Atmospheric Chemistry and Physics*, 14, 10 803–10 822, doi:10.5194/acp-14-10803-2014, <http://www.atmos-chem-phys.net/14/10803/2014/>, 2014.
- 20 Kärcher, B. and Burkhardt, U.: A cirrus cloud scheme for general circulation models, *Quarterly Journal of the Royal Meteorological Society*, 134, 1439–1461, doi:10.1002/qj.301, <http://dx.doi.org/10.1002/qj.301>, 2008.
- Lawson, R. P., Pilon, B., Baker, B., Mo, Q., Jensen, E., Pfister, L., and Bui, P.: Aircraft measurements of microphysical properties of subvisible cirrus in the tropical tropopause layer, *Atmos. Chem. Phys.*, 8, 1609–1620, doi:10.5194/acp-8-1609-2008, 2008.
- 25 Liu, Y. S., Fueglistaler, S., and Haynes, P. H.: Advection-condensation paradigm for stratospheric water vapor, *Journal of Geophysical Research: Atmospheres*, 115, n/a–n/a, doi:10.1029/2010JD014352, <http://dx.doi.org/10.1029/2010JD014352>, 2010.
- 30

- Lohmann, U. and Roeckner, E.: Influence of cirrus cloud radiative forcing on climate and climate sensitivity in a general circulation model, *J. Geophys. Res.*, 100, 16 305, doi:10.1029/95JD01383, 1995.
- McFarquhar, G. M., Heymsfield, A. J., Spinhirne, J., and Hart, B.: Thin and subvisual tropopause tropical cirrus: Observations and radiative impacts, *J. Atmos. Sci.*, 57, 1841–1853, doi:10.1175/1520-0469(2000)057<1841:TASTTC>2.0.CO;2, 2000.
- Mioche, G., Josset, D., Gayet, J.-F., Pelon, J., Garnier, A., Minikin, A., and Schwarzenboeck, A.: Validation of the CALIPSO-CALIOP extinction coefficients from in situ observations in midlatitude cirrus clouds during the CIRCLE-2 experiment, *Journal of Geophysical Research: Atmospheres*, 115, n/a–n/a, doi:10.1029/2009JD012376, <http://dx.doi.org/10.1029/2009JD012376>, 2010.
- Morrison, H., Curry, J. A., and Khvorostyanov, V. I.: A New Double-Moment Microphysics Parameterization for Application in Cloud and Climate Models. Part I: Description, *J. Atmos. Sci.*, 62, 1665–1677, doi:10.1175/JAS3446.1, <http://dx.doi.org/10.1175/JAS3446.1>, 2005.
- Muhlbauer, A., Berry, E., Comstock, J. M., and Mace, G. G.: Perturbed physics ensemble simulations of cirrus on the cloud system-resolving scale, *Journal of Geophysical Research: Atmospheres*, 119, 4709–4735, doi:10.1002/2013JD020709, <http://dx.doi.org/10.1002/2013JD020709>, 2014.
- Muhlbauer, A., Ackerman, T. P., Lawson, R. P., Xie, S., and Zhang, Y.: Evaluation of cloud-resolving model simulations of midlatitude cirrus with ARM and A-train observations, *Journal of Geophysical Research: Atmospheres*, 120, 6597–6618, doi:10.1002/2014JD022570, <http://dx.doi.org/10.1002/2014JD022570>, 2014JD022570, 2015.
- Murphy, D. M.: Rare temperature histories and cirrus ice number density in a parcel and one-dimensional model, *Atmos. Chem. Phys. Discuss.*, 14, 10 701–10 723, doi:10.5194/acpd-14-10701-2014, 2014.
- Podglajen, A., Hertzog, A., Plougonven, R., and Žagar, N.: Assessment of the accuracy of (re)analyses in the equatorial lower stratosphere, *J. Geophys. Res.*, 119, 11,166–11,188, doi:10.1002/2014JD021849, 2014.
- Randel, W. J.: Upper Tropospheric Equatorial Waves In Ecmwf Analyses, *Quarterly Journal of the Royal Meteorological Society*, 118, 365–394, doi:10.1002/qj.49711850409, <http://dx.doi.org/10.1002/qj.49711850409>, 1992.
- Riese, M., Ploeger, F., Rap, A., Vogel, B., Konopka, P., Dameris, M., and Forster, P.: Impact of uncertainties in atmospheric mixing on simulated UTLS composition and related radiative effects, *Journal of Geophysical Research: Atmospheres*, 117, n/a–n/a, doi:10.1029/2012JD017751, <http://dx.doi.org/10.1029/2012JD017751>, 2012.

Skamarock, W. C., Klemp, J. B., Dudhia, J., Gill, D. O., Barker, D. M., G., D. M., Huang, X.-Y., Wang, W., and Powers, J. G.: A description of the Advanced Research WRF Version 3., Tech. Rep., Natl.Cent. for Atmos. Res., 2008.

5 Spichtinger, P. and Krämer, M.: Tropical tropopause ice clouds: a dynamic approach to the mystery of low crystal numbers, *Atmos. Chem. Phys.*, 13, 9801–9818, doi:10.5194/acp-13-9801-2013, 2013.

Stubenrauch, C. J., Cros, S., Guignard, A., and Lamquin, N.: A 6-year global cloud climatology from the Atmospheric InfraRed Sounder AIRS and a statistical analysis in synergy with CALIPSO and CloudSat, *Atmospheric Chemistry and Physics*, 10, 7197–7214, doi:10.5194/acp-10-7197-2010, <http://www.atmos-chem-phys.net/10/7197/2010/>, 2010.

10 Taylor, J. R., Randel, W. J., and Jensen, E. J.: Cirrus cloud-temperature interactions in the tropical tropopause layer: a case study, *Atmos. Chem. Phys.*, 11, 10085–10095, doi:10.5194/acp-11-10085-2011, 2011.

Thompson, G. and Eidhammer, T.: A Study of Aerosol Impacts on Clouds and Precipitation Development in a Large Winter Cyclone, *Journal of the Atmospheric Sciences*, 71, 3636–3658, doi:10.1175/JAS-D-13-0305.1, <http://dx.doi.org/10.1175/JAS-D-13-0305.1>, 2014.

Thompson, G., Rasmussen, R., and Manning, K.: Explicit Forecasts of winter precipitation using an improved bulk microphysics scheme. Part I: Description and sensitivity analysis., *Mon. Wea. Rev.*, 132, 519–542, 2004.

20 Thompson, G., Field, P. R., Rasmussen, R. M., and Hall, W. D.: Explicit Forecasts of Winter Precipitation Using an Improved Bulk Microphysics Scheme. Part II: Implementation of a New Snow Parameterization, *Monthly Weather Review*, 136, 5095–5115, doi:10.1175/2008MWR2387.1, <http://dx.doi.org/10.1175/2008MWR2387.1>, 2008.

Wang, B. and Xie, X.: Low-Frequency equatorial waves in vertically shear flow. Part I: Stable waves., *J. Atmos. Sci.*, 53, 449–467, 1996.

25 Wang, P.-H., Minnis, P., McCormick, M. P., Kent, G. S., and Skeens, K. M.: A 6-year climatology of cloud occurrence frequency from Stratospheric Aerosol and Gas Experiment II observations (1985–1990), *J. Geophys. Res.*, 101, 29407–29429, doi:10.1029/96JD01780, 1996.

30 Wang, T. and Dessler, A. E.: Analysis of cirrus in the tropical tropopause layer from CALIPSO and MLS data: A water perspective, *Journal of Geophysical Research: Atmospheres*, 117, n/a–n/a, doi:10.1029/2011JD016442, <http://dx.doi.org/10.1029/2011JD016442>, 2012.

- Waugh, D. W. and Polvani, L. M.: Climatology of intrusions into the tropical upper troposphere, *Geophysical Research Letters*, 27, 3857–3860, doi:10.1029/2000GL012250, <http://dx.doi.org/10.1029/2000GL012250>, 2000.
- 5 Wernli, H., Paulat, M., Hagen, M., and Frei, C.: Sal—a novel quality measure for the verification of quantitative precipitation forecasts., *Mon. Wea. Rev.*, p. 4470–4487, doi:10.1175/2008MWR2415.1, 2008.
- Winker, D. M., Hunt, W. H., and McGill, M. J.: Initial performance assessment of CALIOP, *Geophysical Research Letters*, 34, n/a–n/a, doi:10.1029/2007GL030135, <http://dx.doi.org/10.1029/2007GL030135>, 2007.
- 10 Wu, L., Su, H., Jiang, J. H., and Read, W. G.: Hydration or dehydration: competing effects of upper tropospheric cloud radiation on the TTL water vapor, *Atmospheric Chemistry and Physics*, 12, 7727–7735, doi:10.5194/acp-12-7727-2012, <http://www.atmos-chem-phys.net/12/7727/2012/>, 2012.

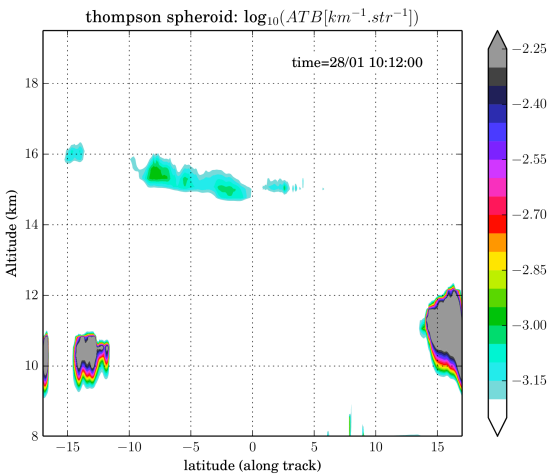
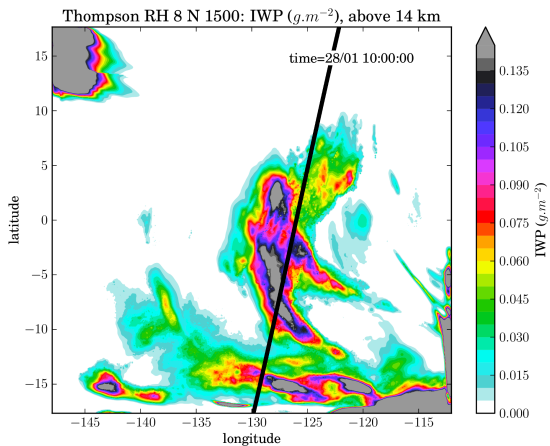
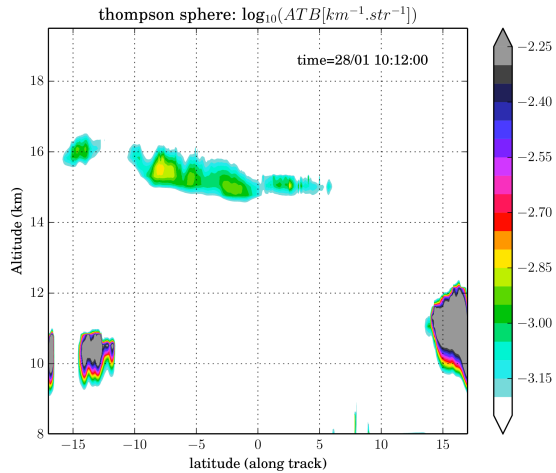
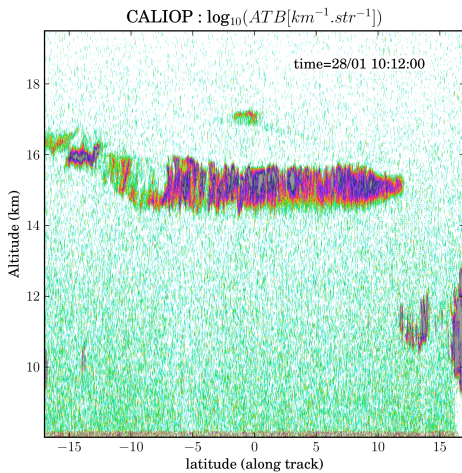


Figure 1. (Top two panels) Decimal logarithm of Total Attenuated Backscatter (ATB) at 532 nm, from (left) CALIOP observations and (right) WRF reference simulation, using default Thompson microphysics, and assuming spherical ice crystals. Total Attenuated Backscatter in the simulation assuming non spherical crystals is also shown (bottom right). (Bottom left panel) : total ice water path above 14 km in the reference simulation, at the time of CALIOP passage. The satellite track is highlighted by the black line.

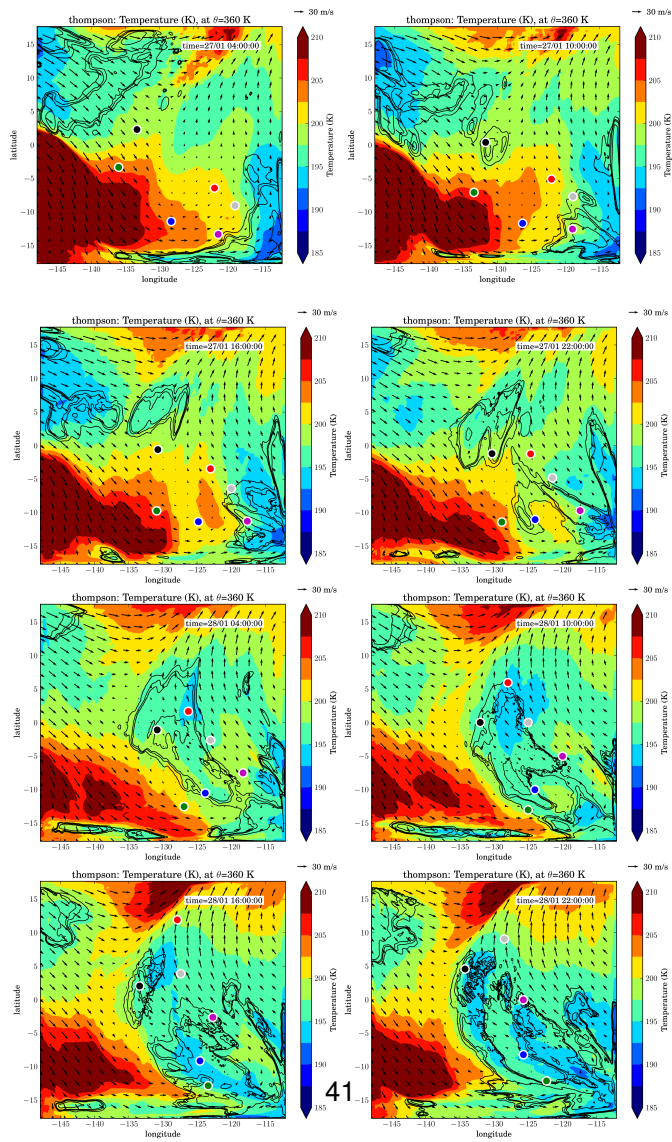


Figure 2. Successive maps of temperature at the potential temperature level $\theta = 360$ K for the reference simulation. The black contours correspond to contours of ice water content of $1.e-8$, $5.e-8$, $1.e-7$ and $5.e-7$ kg.kg^{-1} , respectively. They delimit the cirrus. The color points represent [the position of air parcels surrounding the cirrus on 28/01 at 10:00; they were launched \(backward and forward\) at that date on the isentrope \$\theta = 360\$ K, at the horizontal positions shown by the color points](#). They follow [air-individual 3D-air](#) parcels trajectory and they enlight the air displacement in the region [of the simulation](#). The vectors represent the horizontal winds.

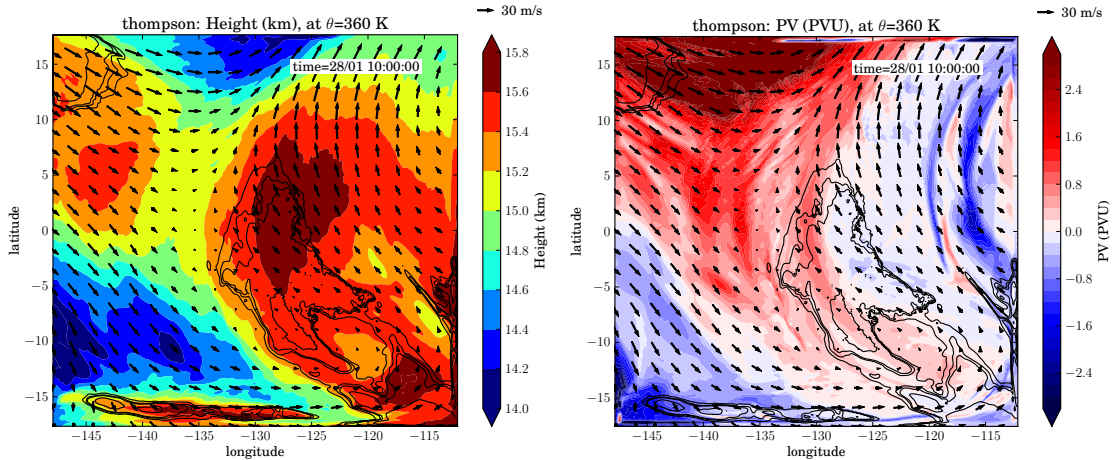


Figure 3. Fields from the reference simulation with Thompson microphysics, on the 360 K isentropic, showing : (Left) Temperature-geopotential height (km, colors) and ice water content (1.e-8, 5.e-8, 1.e-7 and 5.e-7 $\text{kg}\cdot\text{kg}^{-1}$, black contours). (Right) Potential vorticity (PVU, colors) and ice water content. Wind vectors are also displayed.

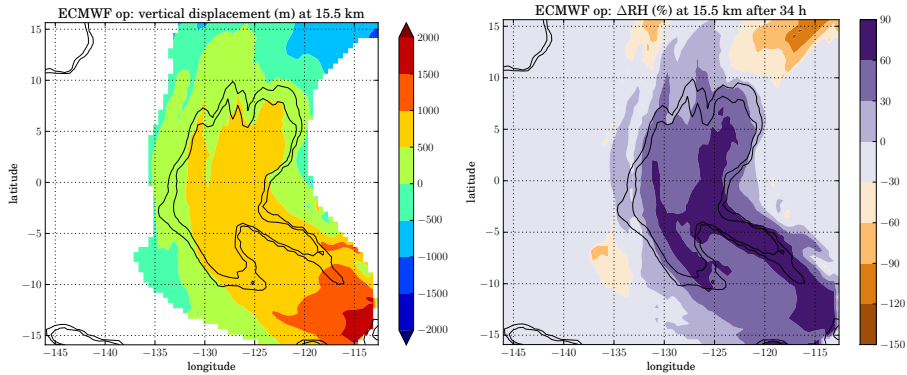


Figure 4. (Left) Lagrangian vertical displacement between the start of the simulation (27 January 2009, 00:00:00 UTC) and 28 January 2009, 12:10:00:00, after 36–34 h of simulation, displayed at the location of air parcels on 28 January, 12:10:00:00 UTC (altitude of 15.5 km). (Right) difference between the initial and "current" Contribution of vertical displacement to relative humidity $\Delta RH = RH_{now} - RH_{ini}$ change ΔRH along a Lagrangian trajectory, see text for details.

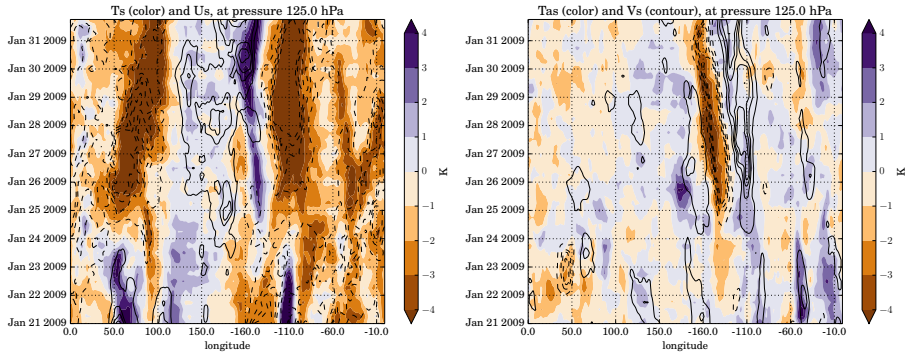


Figure 5. Hovmoeller diagrams of (left) symmetric and (right) antisymmetric temperature anomalies in the ERA interim reanalysis. The averages are computed between 15° North and South and antisymmetric stands for antisymmetric relative to the equator. On the right panel, the black contours correspond to positive (continuous) and negative (dashed) meridional wind anomalies. On the left panel, they correspond to zonal wind anomalies.

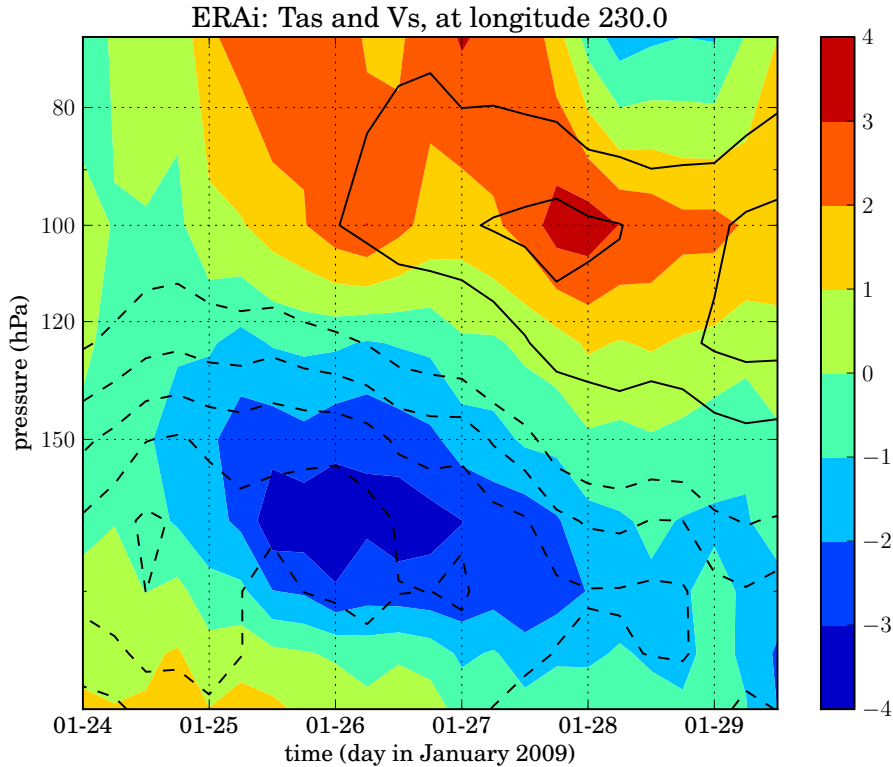


Figure 6. Hovmoeller diagram of symmetric meridional wind (contours, dashed for negative values) and antisymmetric temperature anomalies (color) in the ERA interim reanalysis, before and during the period of the simulation. The averages are computed between 15° North and South and the antisymmetric stands for antisymmetric relative to the equator.

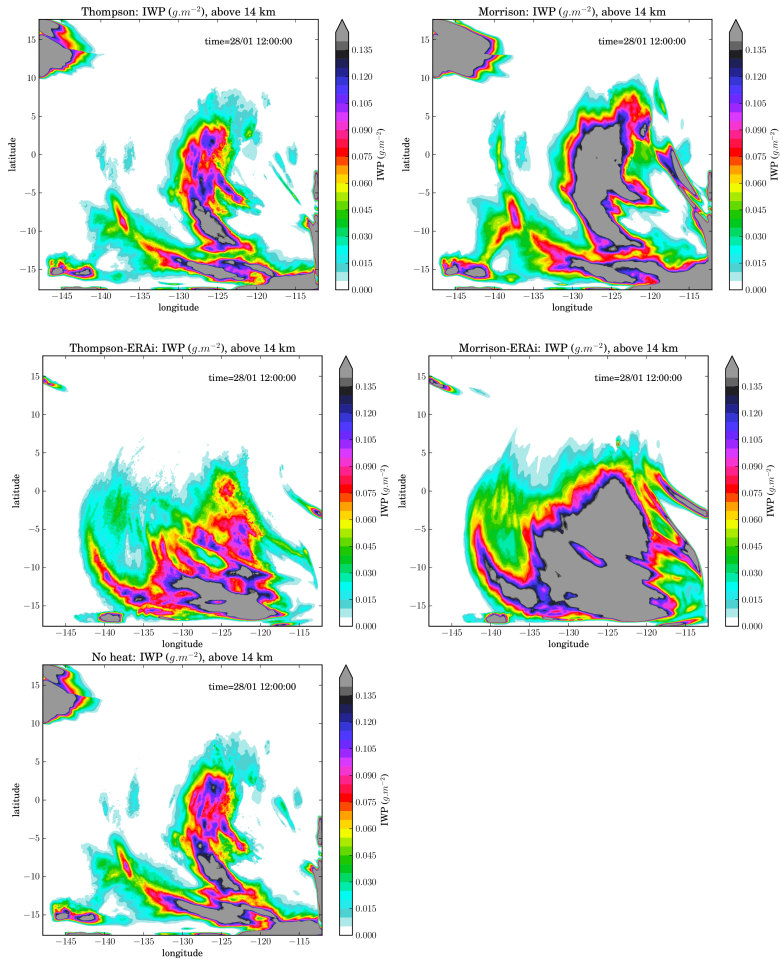


Figure 7. Maps of the Ice Water Path above 14.5 km (vertically integrated ice water content) on 28 January 2009, at 12:00:00 UTC, for ~~in~~ different simulations (see Table 1 for details): (top left) Thompson, (top right) Morrison, (middle left) Thompson-ERAi, (middle right) Morrison-ERAi and (bottom left) No heat.

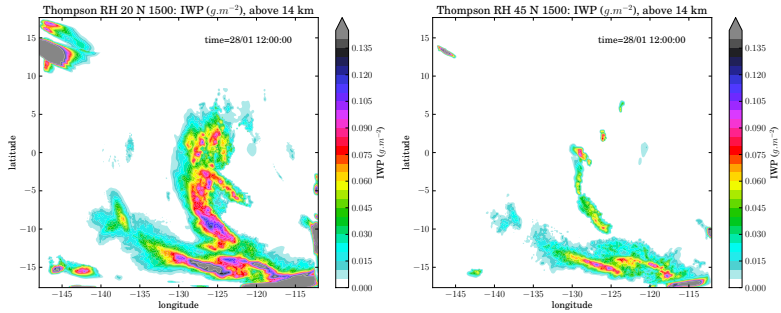


Figure 8. Maps of the Ice Water Path above 14.5 km (vertically integrated ice water content) on 28 January 2009, at 12:00:00 UTC, in simulations using the Thompson scheme with different supersaturation threshold for ice formation (see Sect. 4.3.2 for details): (left) $S_{nuc} = 1.2$ and (right) $S_{nuc} = 1.45$.

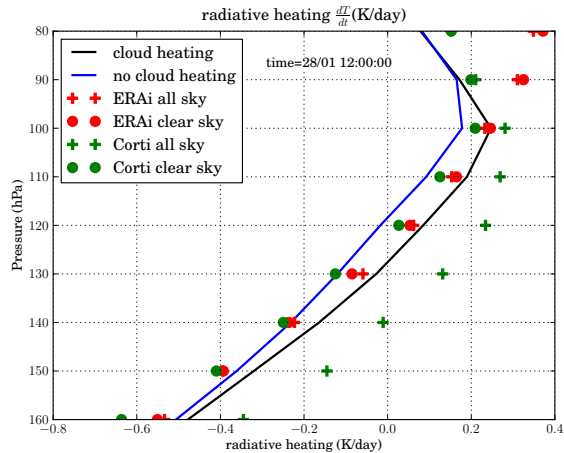


Figure 9. Profiles of radiative heating rates on 28 January 2009, 12:00:00 UTC, in the WRF domain, for the simulations with (black) and without (blue) cloud heating included. For comparison, the three-hours averaged clear sky and all sky radiative heating rates in the ERA interim reanalysis are shown in red, and together with the estimates from Corti et al. (2006) for clear sky and all regions in green.

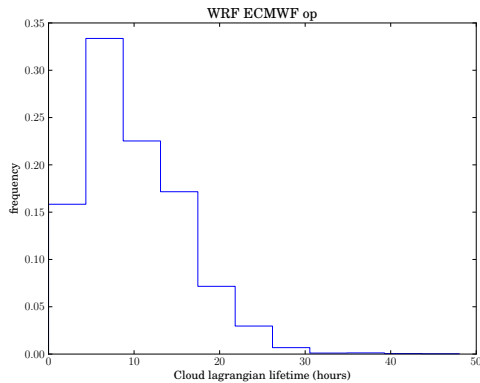


Figure 10. Distribution of in-cloud residence time for air parcels, estimated from Lagrangian trajectories launched on 28 January 2009, 12:00:00 in the reference simulation and calculated forward and backward. Parcels were considered in cloud if the ice water content was bigger than $1.e-10 \text{ kg.kg}^{-1}$.

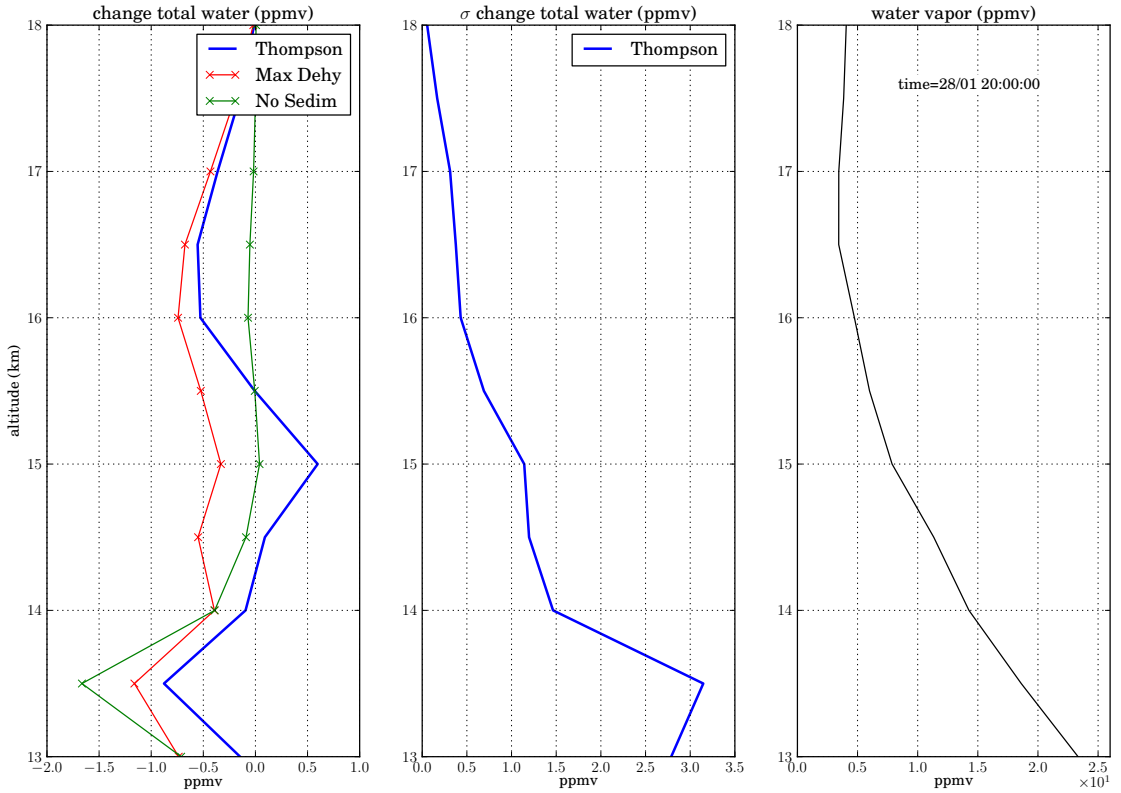


Figure 11. (left) Change in water vapour between the start of the simulation (27 January 2009, 00:00:00) and 28 January 2009, 20:00:00, i.e. after 44 hours of simulation, for three simulations: "Thompson" in blue (Thompson microphysics scheme), "Max Dehy" or "Maximum Dehydration" in red (removal of water vapour above 100% relative humidity), and "No Sedim" or "no sedimentation" in green (sedimentation turned off for temperatures below 220 K). See text for details of the methodology of evaluation of the redistribution. (Middle) [Standard deviation of the water redistribution for the "Thompson" full microphysics case; this emphasizes the variability and uncertainty in the estimate.](#) (Right) Mean water vapour profile in the simulations.

Table 1. List of parametrisations and simulations used in this paper

Simulation name	microphysics	radiation	initial & boundary conditions
Thompson	Thompson	RRTMG	ECMWF op. an.
Thompson-ERAi	Thompson	RRTMG	ERA interim
Morrison	Morrison	RRTMG	ECMWF op. an.
Morrison-ERAi	Morrison	RRTMG	ERA interim
WSM5	WSM5	RRTMG	ECMWF op. an.
No heat	Thompson	RRTMG-no cloud radiative heating	ECMWF op. an.

ECMWF op. an. stands for the European Center for Medium-Range Weather Forecast operational analysis, ERAi stands for the ECMWF interim reanalysis

Table 2. Bulk microphysical properties (ice water content, ice crystal number and effective radius R_{eff}) of the simulated cirrus clouds at 15.5 km on January 28, at 10:00 and values reported from aircraft observations (Lawson et al., 2008).

	WRF Simulation		Lawson et al. (2008)	
	mean	σ	mean	σ
Ice crystal number (L^{-1})	85	131	66	31
R_{eff} (microns)	10.4	1.8	8.8	2.4
Ice water content ($mg \cdot m^{-3}$)	0.10	0.17	0.06	0.1

Table 3. Bulk microphysical properties (ice water content, ice crystal number and effective radius R_{eff} of the simulated cirrus clouds at 15.5 km on January 28, at 10:00, for different choice of the microphysics parameters N_{IN} and S_{nuc} .

$N_{IN}(\#/L)$	150			1500		
S_{nuc}	0.08	0.20	0.45	0.08	0.20	0.45
Ice crystal number (L^{-1})	72	32	9	31	85	9
R_{eff}	10.5	13.8	12.9	10.4	12.6	13.0
Ice water content ($mg.m^{-3}$)	0.09	0.07	0.03	0.10	0.07	0.03

Table 4. Differences in amplitude and in vertical and horizontal centroid location, between the simulated and observed ATB (a proxy for cloud position), along CALIOP track on 28 January 2009, 10 h UTC.

Simulation name	Amplitude	Longitude Latitude along CALIOP track (degrees)	Altitude (m)
Thompson	-0.32	-2.71	-293.
Thompson-ERAi	-1.08	-7.4	80.
<u>Thompson-nested</u>	<u>-1.13</u>	<u>-3.4</u>	<u>-39.</u>
H2O+20%	0.83	-2.9	-820.
Morrison	-0.94	-4.8	401.
Morrison-ERAi	-0.56	-7.1	257.

Table 5. Correlation and SAL (see text for details) for the Ice Water Path [above 14 km](#) in WRF simulations compared to the reference simulation at 12:00:00 on 28 January 2009. The "cloud threshold" for SAL was chosen to be a fourth of the maximum ice water path (see Wernli et al., 2008).

Simulation name	Correlation	Amplitude	Structure	Location
Thompson-ERAi	0.54	0.26	-0.58	0.14
Thompson-nested	0.47	0.36	-1.46	0.20
H2O+20%	0.93	0.34	0.34	0.02
No heat	0.97	0.04	0.29	0.02
WSM5	0.89	0.54	0.14	0.12
Morrison	0.85	0.54	0.46	0.10
Morrison-ERAi	0.62	0.87	1.04	0.08
Thompson-$S_{nuc} = 0.08, N_{LN} = 150$.	0.99	0.036	0.046	0.004
Thompson-$S_{nuc} = 0.20, N_{LN} = 150$.	0.96	-0.32	-0.31	0.02
Thompson-$S_{nuc} = 0.20, N_{LN} = 1500$.	0.96	-0.33	-0.27	0.02
Thompson-$S_{nuc} = 0.45, N_{LN} = 1500$.	0.64	-0.77	-1.30	0.11